# Advances in nanoparticles from gasoline direct injection engines: a focus on physical and chemical characterisation

Xiaochen Wang [a], Wei-Hsin Chen [b,c,d], Jianbing Gao [e, f, *], Yuhan Huang [g]

[a] School of Automobile, Chang'an University, Xi'an, 710064, PR China

[b] Department of Aeronautics and Astronautics, National Cheng Kung University, Tainan 701, Taiwan

[c] Research Center for Smart Sustainable Circular Economy, Tunghai University, Taichung 407, Taiwan

[d] Department of Mechanical Engineering, National Chin-Yi University of Technology, Taichung 411, Taiwan

[e] School of Mechanical Engineering, Beijing Institute of Technology, Beijing, 10081, PR China

[f] Institute for Transport Studies, University of Leeds, Leeds LS2 9JT, UK

[g] Centre for Green Technology, School of Civil and Environmental Engineering, University of Technology Sydney, NSW 2007, Australia

Xiaochen Wang, xc.wang@chd.edu.cn / wangxiaochen510@163.com

School of Automobile, Chang'an University

[*]**Corresponding author:**

Jianbing Gao, gaojianbing@bit.edu.cn / redonggaojianbing@163.com

School of Mechanical Engineering, Beijing Institute of Technology

***Abstract**:* With an increasing market share of gasoline direct injection (GDI) vehicles, high nanoparticulate emissions of GDI engines are of increasing concern due to their adverse impacts on both human health and the ecological environment. A thorough understanding of GDI nanoparticulate properties is required to develop advanced particulate filters and assess the exhaust toxicity and environmental impacts. Therefore, this paper aims to fill this gap by providing a comprehensive review of the physical and chemical characteristics of GDI nanoparticles from a distinctive perspective, including soot oxidation reactivity, morphology, nanostructure, surface chemistry, chemical components, and their correlations. This review begins with a brief description of in-cylinder soot and exhaust particulate features and a comparison between GDI and diesel particulates. Then, the impacts of engine operating parameters and aftertreatments on GDI soot features are discussed in detail. The characteristics of soot particles from oxygenated fuels are introduced. Finally, the conclusions and future research recommendations are presented.

***Keywords**:* Nanoparticles; gasoline direct injection engines; soot oxidation reactivity; nanostructure; surface chemistry; chemical component

Nomenclature

| | | | |
|---|---|---|---|
| AFR | Air/fuel ratio | XRF | X-ray fluorescence spectroscopy |
| bTDC | before top dead centre | XPS | X-ray photoelectron spectroscopy |
| DMC | Dimethyl carbonate | TWC | Three-way catalyst |
| DMF | 2,5-dimethylfuran | ICP-OES | Inductively coupled plasma optical emission spectrometry |
| EC | Elemental carbon | BMEP | Brake mean effective pressure |
| EGR | Exhaust gas recirculation | EEPS | Engine exhaust particle sizer |
| XRD | X-ray diffraction | IMEP | Indicated mean effective pressure |
| GDI | Gasoline direct injection | PAHs | Polycyclic aromatic hydrocarbons |
| VOF | Volatile organics fraction | EDX | Energy dispersive X-ray spectrometer |
| GPF | Gasoline particulate filter | FTIR | Fourier-transform infrared spectroscopy |
| LNT | Lean NO*x* trap | SAXS | Small-angle X-ray scattering |
| OC | Organic carbon | EELS | Electron energy loss spectroscopy |
| PFI | Port fuel injection | DSC | Differential scanning calorimetry |
| PM | Particulate matter | TEM | Transmission electron microscopy |
| PN | Particulate number | HRTEM | *High-resolution* transmission electron microscopy |
| RS | Raman spectroscopy | GC-MS | Gas chromatography and mass spectrometry |
| SCR | Selective catalytic reduction | SEM | Scanning electron microscopy |
| TGA | Thermogravimetric analysis | SMPS | Scanning mobility particle sizer |
| TOC | Thermal/optical carbon | | |

# 1 Introduction

## *1.1 Background*

Nanoparticle emissions from vehicle exhaust cause adverse effects on both human health and the environment. A recent study indicated that each 10 μg/m$^3$ increase in ambient $PM_{2.5}$ concentration was associated with a 0.55-0.74% increase in mortality from all-cause, cardiovascular, and respiratory [1]. In addition, extensive studies also linked the high ambient particulate levels with human health such as lung and cardiovascular diseases, incident brain tumors or even daily mortality [2]. Compared to diesel engines fitted with diesel particulate filters, gasoline direct injection (GDI) engines emit more ultrafine particles (less than 100 nm) [3], of which a high proportion could be deposited in the lung. With the popularity of GDI vehicles in recent years, GDI particulates have become an emerging environmental concern which has prompted the introduction of increasingly stringent particulate regulations. Taking China 6b as an example, the particulate mass (PM) and particulate number (PN) emissions for light-duty gasoline vehicles (Type I test) are limited to 3.0 mg/km and 6.0 × $10^{11}$ #/km, respectively. These regulations have brought the control of ultrafine particulates from GDI engines into sharp focus [4]. Meeting such regulations not only requires engine and fuel co-optimisation but also necessitates the application of gasoline particulate filters (GPFs). To improve the performance of GPFs, a profound understanding of the soot oxidation process are necessary [5, 6].

Numerous studies performed on diesel engines indicate that soot oxidation reactivity depends on its morphology, internal structure and chemical composition [7]. Therefore, a fundamental knowledge of PM characteristics is crucial to developing more effective GPF management systems and extending the catalyst life of GPF. Recently, Al Housseiny, et al. [8] concluded that soot surface chemistry (i.e. oxygen content and the presence of carboxylic acid groups in soot) affected inflammatory and oxidative responses in human lung epithelial cells. In addition, Kwon, et al. [9] reviewed the characteristics of ultrafine particles from engines that are relevant to human health. Polycyclic aromatic hydrocarbons (PAHs), which are the main

organic compounds of exhaust PM, are the genotoxic mutagens that form DNA adducts [10]. The physical and chemical characteristics of soot particles can provide useful information on the PM formation and development of advanced particulate filters and help researchers to assess exhaust toxicity and environmental impacts [6, 11-15].

### *1.2 Soot characterisation methods*

Collection methods may alter the properties of the particulate samples. Therefore, the sampling methods should be carefully selected according to the research purposes and performance of analytical techniques, thus to minimise the test uncertainties. It is recommended that a thermophoretic probe is the most appropriate method for morphological and nanostructural characterisation, whereas a particle trap is the most suitable method for thermal and chemical surface analyses [16].

Soot oxidation reactivity is usually measured using thermal analysis techniques, such as thermogravimetric analysis (TGA) [17, 18] and differential scanning calorimetry (DSC) [5, 19]. With controlled temperature and gas composition during the reaction, TGA measures the variations of the loss of soot mass and DSC measures the energy released by soot oxidation. Based on the measurements, the ignition temperature and activation energy are used to assess the oxidation reactivity of soot samples [20, 21].

Detailed morphological features of soot particles at micro- and nano-scales are observed by transmission electron microscopy (TEM) and *high-resolution* TEM (HRTEM), respectively. Extracted from TEM images, the morphological parameters, including the mean primary particle diameter ($d_p$), the radius of gyration ($R_g$) and fractal dimension ($D_f$), are often used to study the primary particle and agglomerate sizes (see Figure 1a) [22, 23]. As shown in Figure 1c, HRTEM images are widely used to investigate the soot nanostructure by introducing the fringe parameters including fringe length ($L$), tortuosity ($T_f$) and interlayer spacing ($D_s$) [24-26]. Likewise, X-ray diffraction (XRD) provides information on the soot crystallinity which is defined by the interplanar distance between the graphene layers ($d_{002}$), stacking thickness ($L_c$) and crystallite size ($L_a$) (as presented in Figure 1b) [27]. Note that $L$ obtained from HRTEM

may qualitatively agree with $L_a$ obtained from XRD [6]. However, as reported by Guerrero Peña, et al. [28], the crystallite size obtained from XRD is overestimated. In addition, Raman spectroscopy (RS) is frequently used to supplement the information regarding soot nanostructure [29]. Extracted from Raman spectra, the Raman parameters (the intensity/area ratios of bands) are used to study the degree of the order of soot samples [30].

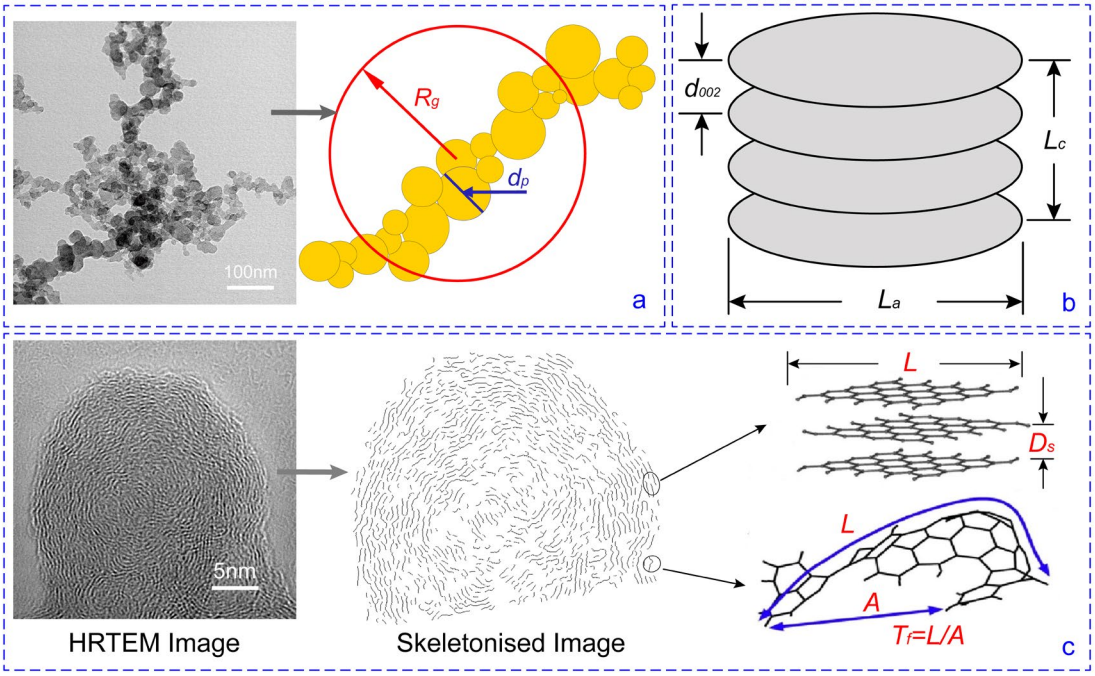


Figure 1. Schematic of morphological features of soot particles at micro- and nano-scales: (a) an agglomerate particle, (b) lattice parameters estimated from XRD spectra (reproduced from Ref. [27]) and (c) fringe parameters from HRTEM images.

Chemical characterisation of PM usually contains the element composition, carbonaceous components (elemental carbon (EC) and organic carbon (OC)) and surface functional groups (SFGs). The most common method to reveal the elemental composition of soot particles may involve scanning electron microscopy (SEM) (or TEM) combined with an energy dispersive X-ray spectrometer (EDX) [31, 32]. The thermal/optical carbon (TOC) analyser is applied to determine the fractions of EC and OC [33, 34]. Regarding soot SFGs, both Fourier-transform infrared spectroscopy (FTIR) and X-ray photoelectron spectroscopy (XPS) are employed [35, 36]. Through both spectra with curve fitting, the concentrations of SFGs, such as aliphatic C-H, hydroxyl group (C-OH) and carbonyl group (C=O), are obtained. PAHs are also evaluated,

which are adsorbed onto the PM or portioned in the semi-volatile PM phase. PAHs are first extracted from PM samples and then analysed using gas chromatography and mass spectrometry (GC-MS) [37-39]. Although the above analytical methods have been commonly used in most publications, some other techniques are also infrequently utilised. Among them, the techniques that are used to characterise soot nanostructure and graphitisation include electron energy loss spectroscopy (EELS), X-ray near edge absorption spectroscopy and small-angle X-ray scattering (SAXS). Moreover, nuclear magnetic resonance, X-ray fluorescence spectroscopy (XRF) and inductively coupled plasma optical emission spectrometry (ICP-OES) are employed to determine the PM's elemental and chemical compositions. Detailed information regarding the fundamentals of these analytical techniques and their applications in soot characterisation is beyond the scope of this work. For further details, the reader is referred to several previous reviews [6, 11, 40-43] and the references therein.

### *1.3 Motivation and outline of this review*

Recently, researchers have conducted numerous experimental and numerical studies to investigate the soot formation mechanisms and mitigation measures. There are a few reviews on the PM and PN emissions from GDI engines. Qian, et al. [44] systematically summarised the PM emissions from modern gasoline-fuelled engines, including the effect of fuel properties, engine operating conditions and driving cycles on PM mass and PN emissions. Additionally, PM and PN emissions in various GDI engines and their control methods to meet the current emission regulations have been presented by Überall, et al. [4], Raza, et al. [45], and Awad, et al. [46]. Although several reviews focused on the features of soot particles from diesel engines [6, 11, 12], a comprehensive summary of soot physicochemical features from GDI engines is still absent given GDI soot is attracting more and more attention. Moreover, GDI soot has significant differences with diesel soot in physicochemical features and the correlations among these features.

Therefore, this paper aims to fill this gap by providing a comprehensive review of the physical and chemical characteristics of GDI soot particles. This study will focus on

physicochemical features, including soot oxidation reactivity, soot morphology and nanostructure, graphitisation degree, chemical composition, and surface chemistry. Although the above features are imperative to characterise GDI PM, they cannot be fully examined due to the limited technique accessibility. Consequently, the present review tries to build a whole picture of GDI soot features based on vast experimental investigations. The remaining of this paper is organised as follows. First, Section 2 introduces the PM characteristics of GDI engines, including both in-cylinder and exhaust soot, and the comparisons between the properties of GDI and diesel exhaust particulates. Next, Section 3 systematically describes the effects of engine operating parameters on the characteristics of GDI PM, including engine speed and load, equivalence ratio, fuel injection strategies and exhaust gas recirculation. Then, Sections 4 discusses in detail the effects of the application of exhaust after-treatment technologies on GDI PM characteristics, namely three-way catalyst (TWC) and GPF. Finally, the conclusions and future perspectives are presented. This review is expected to provide a thorough understanding of GDI soot properties which are critical for the assessment of health and environmental impacts of GDI nanoparticles and the development of effective mitigation measures.

# 2 PM characteristics of GDI engines

## *2.1 In-cylinder soot features*

The formation of soot particles in combustion engines involves complex physical and chemical processes, including fuel pyrolysis, nucleation, coalescence, surface growth, agglomeration and oxidation [44, 47]. The evolution of in-cylinder soot structure can provide useful information on the actual soot formation process inside the engine combustion chamber [48]. For this purpose, Kook et al. [49-52] developed a novel in-cylinder soot sampling system in an optical wall-guided GDI engine. Unlike other studies which used optical diagnosis [53] and numerical simulation [54] methods, they used TEM images of the sampled particles to characterise their morphology and internal nanostructure, which provided detailed information regarding the in-cylinder soot status.

TEM images showed that in-flame soot exhibited chain-like and/or ring shapes, and the

samples that were located on the exhaust valve side had a higher particle concentration and larger primary particles and agglomerates than those located on the intake valve side [49]. As shown in the natural flame luminosity images, those on the exhaust valve side were surrounded by wall wetting-induced poor fire, which persisted for a longer period. Therefore, longer soot residence time enhanced soot surface growth and aggregation, thus leading to larger primary particles and agglomerates [49]. Subsequently, the changes in the morphology of the in-flame particles were investigated under piston- and liner-wetting conditions, which were obtained from the selected start of the injection (SOI) of 320 °CA and 180 °CA before top dead centre (bTDC), respectively. The results showed that early injection with piston-wetting produced soot particles with a larger gyration radius and primary particle diameter, lower fractal dimension and a more graphited structure, which was indicated by a longer fringe length, less tortuosity and smaller layer spacing compared to the later injection with liner wetting, as shown in Table 1 [50]. These phenomena can be explained by the fact that the soot particles that were collected from the piston-wetting condition suffered a longer residence time, which led to a more carbonised structure.

Table 1. Quantitative analysis of in-cylinder soot morphology and nanostructure under various wall-wetting conditions (data from Ref. [50]).

| Average values of structural parameters | Wall-wetting conditions | |
|---|---|---|
| | Piston-wetting (SOI = 320°CA bTDC) | Liner-wetting (SOI = 180°CA bTDC) |
| $d_p$ | 23.91 ± 0.24 nm | 22.01 ± 0.19 nm |
| $R_g$ | 68.55 ± 3.33 nm | 60.82 ± 1.93 nm |
| $D_f$ | 1.69 | 1.71 |
| $L$ | 1.01 ± 0.02 nm | 1.00 ± 0.01 nm |
| $T_f$ | 1.18 ± 0.01 | 1.19 ± 0.01 |
| $D_s$ | 0.405 ± 0.002 nm | 0.432 ± 0.001 nm |

Note that in Refs. [49-52], three to seven injection cycles (i.e. firing cycles) were adopted for each sampling run, and the soot was directly deposited onto the TEM gird surface due to the thermophoretic force. Therefore, the time-sequential in-cylinder soot features are missing. This problem can be addressed by the total cylinder sampling system [55], which has long been applied in diesel engines [56]. At a predetermined sampling crank angle, the electronic control unit cut diaphragms in the engine cylinder head. This allows the in-cylinder gas to escape

rapidly out of the combustion chamber into a sampling bag, which is pre-filled with nitrogen [57]. With this sampling apparatus, the evolution of in-cylinder diesel soot features in various combustion phases has been widely analysed [36, 58, 59]. Therefore, further research is necessary to reveal the in-cylinder GDI soot features as a function of the crank angle by combining the total cylinder sampling system in GDI engines and multiple analytical techniques, especially for soot chemical features.

### *2.2 Exhaust particulate features*

Compared to in-flame soot, exhaust soot showed a lower fringe separation and more defined core-shell boundaries at both injection pressures [51], which means that exhaust soot is more difficult to oxidise than in-cylinder soot. The result is in agreement with the subsequent work of the authors [50, 52], who reported that exhaust soot exhibited a longer fringe length, smaller fringe tortuosity and fringe separation. This indicates a more ordered nanostructure, regardless of injection timing and test fuel.

GDI soot reactivity is a key factor that affects GPF regeneration behaviour. Soot with higher reactivity is easier to oxidise, which benefits GPF regeneration. Generally, soot reactivity is inherently governed by its physicochemical features. As soot reactivity is often evaluated by the TGA methodology, it is influenced by the heating program, oxidising conditions and sample load [60, 61]. There are many examples of soot oxidation kinetics in the literature. According to Hu, et al. [62], the activation energy of soot particles derived from the worldwide harmonised light-duty vehicle test cycle (WLTC) was in the range of 91 kJ/mol–133 kJ/mol, depending on the oxidation temperature and calculated methodology. In Ref. [63], the activation energy of soot samples that were collected at five different engine conditions ranged from 125 kJ/mol to 142 kJ/mol.

TEM images show that GDI exhaust particles can be classified into the following two groups: carbonaceous particles and non-carbonaceous particles [64]. The former usually exhibits cluster-like and chain-like soot [64], while the latter contains Ca-rich, S-rich, Fe-rich and Zn-rich particles, with morphologies of nearly circular, irregular and prismatic shapes [31].

177 It is worth noting that ultrafine ash particles are in almost equal amounts to or higher than soot
178 particles, which maybe because a large amount of soot that is generated in the combustion
179 chamber tends to form soot agglomerates that are larger than 100 nm [31]. This result suggests
180 that the larger amount of ash in ultrafine particles should be taken into consideration to evaluate
181 their environmental and human health effects. As ash particles mainly originate from the in-
182 cylinder consumed lubricating oil, Seong, et al. [65] identified engine oil-derived ash
183 nanoparticles by dosing various formulated engine oil into the fuel system of a GDI engine.
184 The STEM results showed that ash particles exist as single or multi-agglomerated forms and
185 are separated from or deposited on aggregated soot.

186 Generally, HRTEM images reveal that GDI exhaust soot exhibits the core-shell
187 nanostructure and presents a more graphited structure than in-cylinder soot. Moreover, the
188 primary particles with an outer shell that is interrupted by multiple cores were observed, which
189 infers that in the combustion chamber, an abundant growth of nuclei and the coalescence of
190 soot may simultaneously occur before each core grows into a primary particle [66]. In addition
191 to the core-shell structure (also regarded as a 'mature' structure), a small number of amorphous
192 particles (i.e. an isotropic graphite crystalline but with no obvious graphene layers) and
193 disordered particles (i.e. no crystalline structure) were observed [37].

194 Regarding the element components, an EDX analysis of soot particles emitted from a GDI
195 vehicle (Euro V) over the WLTC shows that the main components are C and O, followed by S,
196 whereas the minor components include Ca, P, Na, Si, Zn (mainly from lubricating oil) and Fe
197 (mainly from engine wear) [67]. This is generally consistent with another study [68], which
198 identified using inductively-coupled plasma mass spectrometry that the emission factors of the
199 main elements in PM can be ordered from high to low as follows: S > Fe > Ca > Al > P > Na.
200 As reported in Ref. [69], under the WLTC, the particulate-PAH emissions from GDI vehicles
201 were 4.8 ± 1.4 μg/km, which is three orders of magnitude higher than those from PFI vehicles.
202 Moreover, the benzo [a] pyrene (BaP) emission factors for GDI vehicles were 4.3 times higher
203 than those for PFI vehicles.

Figure 2 shows particle and gas phase processes of diesel engine particulate matter emissions into the atmosphere. Particulates from the engine exhaust valve into the atmosphere involve the exhaust system, the aftertreatment devices, the dilution tunnel and the atmosphere. Along the exhaust pipe, the changes and/or reactions occur in sequence, including oxidation, agglomeration and thermophoresis in the exhaust system and the physical removal and chemical reactions in the aftertreatment devices. After exiting the exhaust pipe, the particle processes cover HC adsorption and condensation; nucleation in the dilution tunnel; and diffusion and continuous dilution in the atmosphere [70, 71]. Although the effect of implementing TWC and GPF on soot features has been partly studied, studies on variations in soot features along the entire exhaust path of GDI engines are limited (see Section 3.2). Previously, Gao, et al. [72] found that diesel PM collected at different tailpipe positions has different physicochemical properties. However, the change in the GDI particulate features as a function of the exhaust distance and local temperature is unknown. Regarding the particle processes that occur in the dilution tunnel and the subsequent atmosphere, the soot morphology and chemical composition may change significantly due to both transport and physical removal processes and chemical transformations [73]. Therefore, the differences in GDI soot features from the exhaust valve into the atmosphere must be clarified in the future.

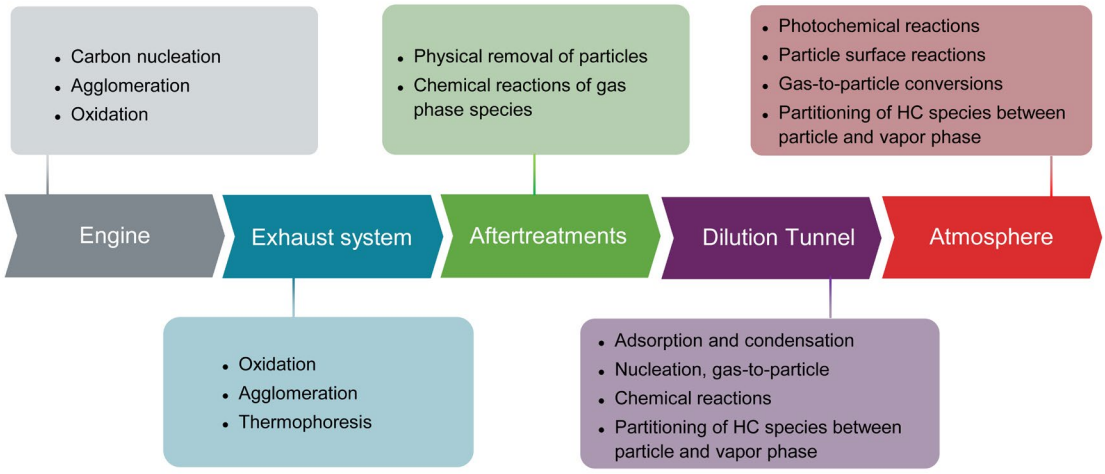


Figure 2. Schematic of the particle and gas-phase processes of diesel engine PM emissions into the atmosphere (reproduced from Ref. [71]).

### *2.3 Comparisons between GDI and diesel particulates*

Under the high combustion temperature and pressure conditions in both GDI and diesel engines, some similarities in the soot features are expected between diesel and GDI exhaust particles. However, the physicochemical features of soot particles from GDI and diesel engines have some inherent differences in terms of morphology, nanostructure, chemical components and oxidation reactivity due to the differences in the fuel properties, mixture formation strategies, ignition and combustion processes. Therefore, a comparison between diesel and GDI exhaust particles is made by checking their similarities and differences regarding soot reactivity and its related features.

Through TGA, Oo, et al. [74] identified that GDI exhaust soot had a faster oxidation process and a lower oxidation temperature, which demonstrates that it is easier to oxidise than diesel exhaust soot. This is in good agreement with the observation of Wang-Hansen, et al. [75]. The more reactive nature of GDI soot indicates that it may be advantageous to the regeneration of the particulate filter. Note that both studies on the comparison of soot oxidation were performed under a given atmosphere. However, the exhaust environments for GDI and diesel engines are different. For example, GDI engines with stoichiometric combustion have lower $O_2$ concentrations in the absence of $NO_2$ downstream of a three-way catalyst (TWC) compared to diesel engines. Therefore, a further comparative study on soot oxidation for both engines could be conducted under each exhaust-like gas atmosphere.

Concerning soot morphology, TEM images showed that diesel particulate was composed of nearly all aggregates while GDI particulate was composed of a complex mixture of aggregates covering single spheroids, nascent soot, and irregular soot [76]. As observed by Gaddam [77], the GDI soot was ‘open and chain-like’, whereas the diesel soot was more like a ‘compacted assembly’. The differences in morphology can be verified by the morphological parameters. The author pointed out that the $D_f$ of the gasoline soot was 2.03, which was lower than that of diesel soot with 2.39. This means that the GDI soot agglomerates exhibit a less compact and more branched morphology [77]. However, Lu, et al. [78] identified using SEM

that the $D_f$ of the soot sample from the gasoline vehicle was 1.769 ± 0.006, which lies in between that of particulates from the heavy-duty diesel vehicle (1.752 ± 0.014) and light-duty diesel vehicle (1.789 ± 0.076). In addition, in Ref. [79], the $D_f$ of the diesel particulates was within the range of 1.70–1.90, whereas that of the GDI particulates was located in wider distribution, ranging from 1.45 to 2.21. Unlike $D_f$, GDI soot often exhibits a smaller mean primary particle diameter than diesel soot [74, 79, 80].

Regarding the nano-scale level, HRTEM images reveal that GDI soot presents a more amorphous and disordered structure, whereas diesel soot shows a more graphitic and organised morphology [66, 77]. Likewise, the skeletonised images show that the GDI soot contains more irregularly patterned, shorter and more curved fringes than diesel soot [81]. Correspondingly, a shorter fringe length [74, 77] and larger tortuosity and interlayer spacing [79] were observed for the GDI particulate samples. In contrast to diffusion combustion in diesel engines, it is speculated that premixed combustion in GDI engines provides fewer hydrocarbons and carbon in the soot formation process, thus decreasing the graphitisation of particles. Additionally, the difference in fuel properties between gasoline and diesel, particularly the content and species of aromatic hydrocarbons, may partly account for the observation. Compared to diesel fuel, gasoline contains a larger proportion of smaller PAHs, with less electronic stabilisation and thermodynamic stability. During fuel pyrolysis, smaller PAHs tend to produce $C_2$ fragments and further PAHs containing five-membered rings, and the latter has a more curved nanostructure [82]. The less-ordered structure of GDI soot agrees with the higher soot oxidation reactivity obtained from TGA.

Regarding the elemental composition, Oo, et al. [74] determined through TEM-EDX that GDI soot had a lower fraction of carbon but a higher percentage of oxygen than diesel soot. As analysed by XRF, the particulate sample that was collected from a GDI vehicle contained more oil additive elements, such as P, Ca, Zn, and wear metals, such as Fe and Al, compared to a diesel vehicle [80]. The XPS results show that only C, O and N are detected in diesel soot, whereas additional inorganic elements, such as S, P and Zn, are observed in GDI soot [80]. Regarding PAH emissions, the patterns of PAHs of GDI vehicles are similar to those of diesel

vehicle, considering the larger numbers of nanoparticles and the adsorbed genotoxic PAHs. Furthermore, note that the sum of 16 US Environmental Protection Agency (EPA) priority control PAHs in GDI exhausts (without GPF) is higher than that in diesel exhausts (equipped with DPF) [38]. The result implies that GDI vehicles would need particulate filters to reduce both nanoparticles and genotoxic PAHs.

Figure 3 illustrates the differences between GDI and diesel particulates. The three differences are summarised as follows: i) GDI soot is generally more reactive and easier to oxidise than diesel soot; ii) GDI soot exhibits smaller primary particles with a less-ordered nanostructure than diesel soot, whereas the trend in fractal dimension is not conclusive; and iii) GDI soot contains more inorganic and metallic elements (such as P, Ca and Zn) than diesel soot, which originate from lubricating oil additives and engine wear.

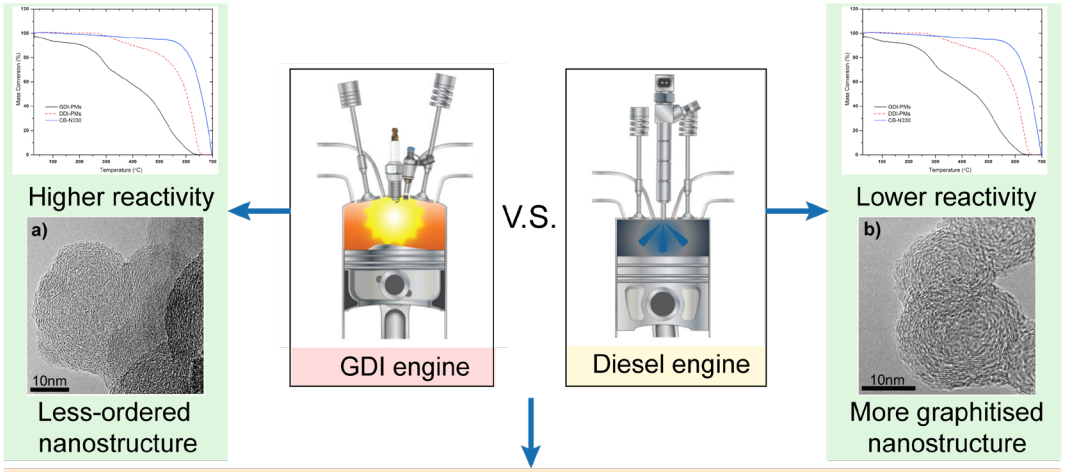


XRF results

| Element [%] | Fe | Ca | P | Zn | Cr | Ni | Cu | Al |
|---|---|---|---|---|---|---|---|---|
| GDI soot | 4.70 | 4.19 | 2.06 | 1.89 | 0.82 | 0.52 | 0.17 | 0.13 |
| Diesel soot | 0.061 | 0.038 | 0.029 | 0.024 | 0.003 | 0.004 | 0.004 | 0.004 |

GDI soot contains more inorganic and metallic elements than diesel soot.

Figure 3. Differences between GDI and diesel particulates (TG curves and XPF results were from Oo, et al. [74], TEM images were from Uy, et al. [80]).

## 3 Influences of engine operating parameters on GDI soot features

Various engine operating parameters influence the in-cylinder combustion conditions and

exhaust atmosphere, which can affect the physicochemical characteristics of GDI exhaust particles. Many studies have investigated the impact of operating conditions on soot features. This section focuses on this topic in detail.

### *3.1 Engine speed and load*

Choi, et al. [63] evaluated the soot oxidation reactivity of GDI particulates generated at the cold-idle and the following two different steady-state conditions: 1250 r/min-25% load and 1500 r/min-50% load. In contrast to diesel soot, variations in GDI soot reactivity are less sensitive to the engine operating point. The authors explained that in GDI engines, flame propagation combustion provides a more consistent in-cylinder fuel-air mixture and flame temperature conditions, irrespective of the engine load and speed, which is different from the nature of diffusion combustion in diesel engines. In addition, they ascribed the differences in GDI soot reactivity to the changes in organic fractions and ash content with the various operating conditions rather than the soot structure. However, other studies [39, 83] found that soot that is produced at a higher engine load is more difficult to oxidise.

Collected at various operating points, agglomerated particles exhibit similar morphology with a chain-like structure that comprises a few to hundreds of primary particles [81, 84]. However, the trends regarding the primary particle size with the change in engine load are conflicting. Seong, et al. [81] observed that the mean primary particle diameter increased from 20 nm to 29 nm, as the engine load increased from 25% to 75% at the speed of 1500 r/min. Likewise, Gaddam, et al. [84] found that elevated engine load (increasing fuel quantity from 11 mg/cycle to 21 mg/cycle) increased the primary particle size from 21 nm to 25 nm and resulted in a larger gyration diameter and fractal dimension. However, Sharma, et al. [85] reported that the mean primary particle diameter of gasoline soot decreased from 31.22 nm to 20.57 nm when the load was increased from 50% to 100%. The authors explained that a higher maximum in-cylinder temperature at higher load conditions leads to the predominance of particle oxidation over particle nucleation.

Figure 4 presents the HRTEM images of GDI soot collected at various operating points

[63]. Visually, the three samples have the typical core-shell nanostructure, as the inner core contains fringes with random orientations, and the outer shell is composed of parallel and concentrically oriented lamellae. Additionally, the visual examination reveals that similar orders of crystalline structures are observed amongst the three samples. In particular, in the cold-idle condition, the soot particle presents a clear concentric fringe pattern. Although the Raman Spectra further validates that GDI particulate samples have a similar soot nanostructure, irrespective of engine operating points, no fringe parameters that were extracted from the HRTEM images were quantified [63]. Quantitative fringe parameters from another work [77] show that soot that is generated at a high load (fuel quantity = 21 mg) has a shorter fringe length but a larger fringe tortuosity than soot collected at a low load (fuel quantity = 11 mg). However, the fringe discrepancies in both conditions are slight. Zhang, et al. [86] pointed out that the interlayer spacing of idle soot was the largest, followed by the soot sample at the cold start condition. In addition, the interlay spacing of soot particles increased when the engine load increased from 3 bar to 7 bar brake mean effective pressure (BMEP) at the fixed engine speed of 2000 r/min, whereas it slightly decreased when the engine speed increased from 1200 r/min to 2000 r/min at the fixed engine load of 5 bar BMEP. The fringe analysis from Ref. [77, 86] indicates that an elevated engine load emits soot particles with a less-ordered nanostructure. Interestingly, this trend contradicts the commonly accepted result of diesel soot that higher engine loads lead to a more ordered nanostructure due to the higher temperature, more fuel-rich regions and longer diffusion combustion phase [87, 88].

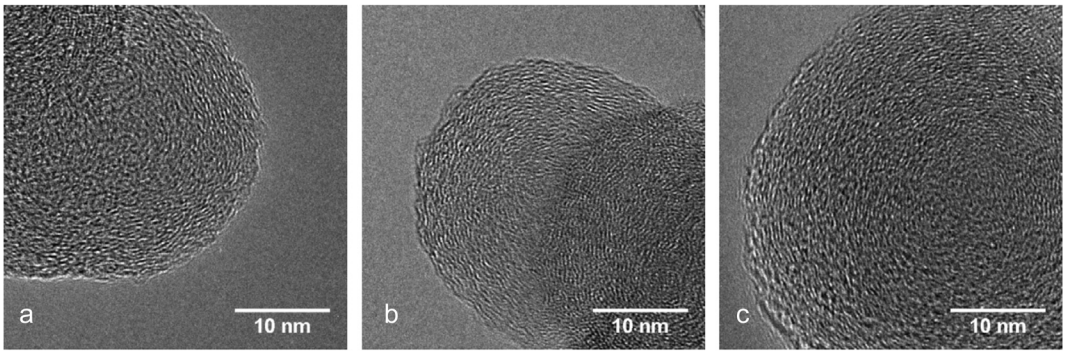


Figure 4. HETEM images of GDI soot collected at: (a) cold-idle; (b) 1250 r/min-25%; and (c) 1500 r/min-50% (adapted from Ref. [63]).

Regarding the chemical composition, the PM sample that was collected at the cold-idle condition has a much higher volatile organics fraction (VOF) compared to those generated in hot steady-state conditions [63]. When the engine load increases, the VOF generally decreases, while the soot faction increases [39, 64]. This is because a higher engine load operation induces a higher exhaust temperature, and more volatile organic compounds are emitted in gas-phase forms rather than particle-phase forms. As indicated in Ref. [37], when the engine load is increased from 60 N·m to 120 N·m, the vapor-phase PAHs with two, three and four rings and the particulate-phase PAHs with four, five and six rings gradually increased, especially for the two-ring PAH. Under the high engine load of 120 N·m, the peak concentrations of PAHs were found at the engine speed of 2000 r/min. When the engine was operating at 60 N·m, the minimum values were found at 2500 r/min.

### *3.2 Equivalence ratio*

The equivalence ratio is an important parameter governing engine particle emissions due to its influence on both the oxygen concentration and the combustion temperature. With the increasing equivalence ratio, more fuel availability may result in higher soot surface growth rates, along with the restrain of soot oxidation caused by the lower in-cylinder oxygen concentration [89]. Moreover, the higher in-cylinder temperature under fuel-rich conditions may improve both the particle surface growth and oxidation. These in-cylinder changes may alter the soot features.

According to the previous studies [79, 84], there is no consensus regarding the impact of the equivalence ratio on agglomerates and primary particle sizes. Wu, et al. [79] reported that the soot particles that were collected at the air/fuel ratio (AFR) of 14.7 had the highest $D_f$ and $D_p$, which reveals that particulate samples under stoichiometric conditions exhibit the most compactly clustered agglomerates with the largest primary particle size. They further stated that under the fuel-rich condition (AFR = 13), the reduced $d_p$ was caused by the predominant effect of particle oxidation because of the high temperature. However, under the fuel-lean conditions (AFRs = 16 and 18), thanks to the excess air, enhanced particle oxidation reduced the primary

372 particle size. In contrast, in Ref. [84], it was pointed out that with the increasing AFR, the mean
373 primary particle diameter increased from 19 nm to 23 nm. Endo, et al. [90] found that soot from
374 a pool fire on the wall surface exhibits a larger primary particle diameter, whereas that from
375 bulk-gas in the cylinder tends to be smaller in size, which is consistent with the results in Ref.
376 [49]. Furthermore, the authors found that a larger proportion of large particles can be observed
377 for fuel-rich combustion (ARF = 12.5), which indicates that the pool fire soot is dominant.
378 However, Seong, et al. [91] pointed out that $d_p$ exhibited no statistically significant changes
379 with an equivalence ratio from 0.98 to 1.13. The authors explained that for various equivalence
380 ratios, the spark timings were adjusted in the experiments to keep the same CA50 (the crank
381 angle at which 50% of the cumulative heat is released).

382 Like primary particle size, the effect of the equivalence ratio on soot nanostructure is
383 inconclusive. At a nanoscale level, particulate samples from various equivalence ratios present
384 the typical shell-core structure with different degrees of graphitisation. Table 2 shows the
385 average values of soot nanostructual parameters versus AFR obtained from HRTEM. As
386 reported by Gaddam, et al. [84], soot from fuel-rich combustion (AFR = 13) displayed a more
387 amorphous structure, with the smallest fringe length but largest tortuosity amongst three
388 samples from AFRs of 17, 15 and 13. In addition, no obvious differences in the soot
389 nanostructure were observed between stoichiometric (AFR = 15) and fuel-lean (AFR = 17)
390 conditions. However, according to Wu, et al. [79], the particulate sample that was generated
391 under the stoichiometric condition showed the shortest fringe length, largest fringe tortuosity
392 and smallest fringe separation distance. Their results of the $sp^2/sp^3$ ratio that was obtained from
393 the XPS supported the HRTEM observation that soot particulates with a stoichiometric
394 operation exhibited a more disordered nanostructure. The authors further attributed the different
395 trends in soot structure to the different engine configurations and test fuel properties. From a
396 fundamental perspective, it can be hypothesised that increasing the equivalence ratio results in
397 more fuel but lower oxygen availability, which leads to higher carbonisation and a more ordered
398 structure. However, at the same time, a higher in-cylinder temperature caused by a higher
399 equivalence ratio affects both soot carbonisation and oxidation. Therefore, to clarify the effect

of the equivalence ratio on soot nanostructure, it should be combined with computational fluid dynamics (CFD) [92] or in-cylinder optical diagnostics (such as spatiotemporal flame luminosity [93]) to determine the combustion characteristics that are related to soot formation and oxidation.

Table 2. Soot nanostructural parameters versus AFR obtained via HRTEM.

| Reference | Engine type | Operating point | Sampling method | AFR | Nanostructural parameters | | |
|---|---|---|---|---|---|---|---|
| | | | | | $L$ (nm) | $T_f$ | $D_s$ (nm) |
| Gaddam, et al. [84] | single cylinder, 549 cc, 11.97:1 | n = 2100 r/min, fuel quantity = 11 mg/cycle | thermophoretic sampling | 13 | 0.72 | 1.210 | - |
| | | | | 15 | 0.82 | 1.175 | - |
| | | | | 17 | 0.80 | 1.176 | - |
| Wu, et al. [79] | 4-cylinder, 1.498 L, 12:1 | n = 2000 r/min, fuel quantity = 46.3 mg/cycle–49.3 mg/cycle | Dilution sampling | 13 | 0.91 | 1.46 | 0.39 |
| | | | | 14.7 | 0.83 | 1.49 | 0.38 |
| | | | | 16 | 0.87 | 1.47 | 0.40 |
| | | | | 18 | 0.85 | 1.44 | 0.41 |

The results that are derived from the FTIR showed that soot produced at fuel-rich combustion had significant organic content, which indicates that soot oxidation requires lower activation energy [77, 84]. However, Zelenyuk, et al. [94] determined that fuel-rich combustion increased the particulate mass with a higher EC than fuel-lean combustion. The authors stated that the number of fractal EC particles increased when the equivalence ratio was increased from 0.90 to 2.10, which indicates a more incomplete combustion. In addition, more than 90% of EC-dominated particles are observed for the lean stratified (2000 r/min, 2 bar BMEP, and $\lambda$ = 2.10) condition, whereas PM from the lean homogeneous (2000 r/min, 4 bar BMEP, and $\lambda$ = 1.54) operation contains a relatively large fraction of organic particles, which are mainly composed of heavy alkanes and alkenes. This observation agrees with the results in Ref. [95], where the experiments were operated in lean-stratified, lean-homogeneous and stoichiometric modes. The results showed that pre-GPF PM in the lean-stratified mode had the largest EC, whereas the lean-homogeneous mode had the largest OC.

Lean GDI combustion can effectively increase fuel economy and reduce $CO_2$ emissions. However, the focus should be placed on both PM and PN emissions control under lean operations, especially under stratified-lean GDI combustion [95, 96]. In addition, the above

discussions reveal that there are inconsistent opinions regarding the effect of the equivalence ratio on soot morphology and nanostructure. Therefore, more work is required to comprehensively characterise the soot particulates from lean GDI combustion.

### *3.3 Fuel injection pressure*

For pre-mixed flames in GDI engines, soot formation is dependent on the quality of fuel/air mixing. Therefore, fuel injection parameters, including injection timing and pressure, significantly affect the time available for premixing, fuel evaporation and fuel impingement, thereby influencing soot formation and oxidation [97]. Increasing the fuel pressure reduces the diameter of the fuel droplets, which improves atomisation and results in a more homogenous fuel-air mixture. However, it is worth noting that an over-high injection pressure increases spray penetration length, which may increase the opportunity of fuel impingement [45].

Koch, et al. [98] studied the variations in soot oxidation regarding the pressure changing from 50 bar to 150 bar. The derivative thermogravimetry (DTG) results showed that a higher oxidation temperature (defined as the temperature at the maximum oxidation rate [$T_{max}$]) was observed for the injection pressures ($P_{inj.}$) of 50 bar and 75 bar, which indicates a lower oxidation reactivity. However, the soot samples that were generated at $P_{inj.} > 87.5$ bar presented a lower $T_{max}$ (approximately 525 ºC), which reveals that they are more reactive regarding oxidisation. Similarly, Easter [99] identified using both isothermal and non-isothermal tests that soot for $P_{inj.} = 60$ bar was more reactive regarding oxidisation than that for $P_{inj.} = 20$ bar (non-isothermal test results were shown in Figure 6a). The trend is consistent with the fact that a higher oxidation reactivity of diesel particulates was obtained at the higher injection pressure conditions [11, 100, 101].

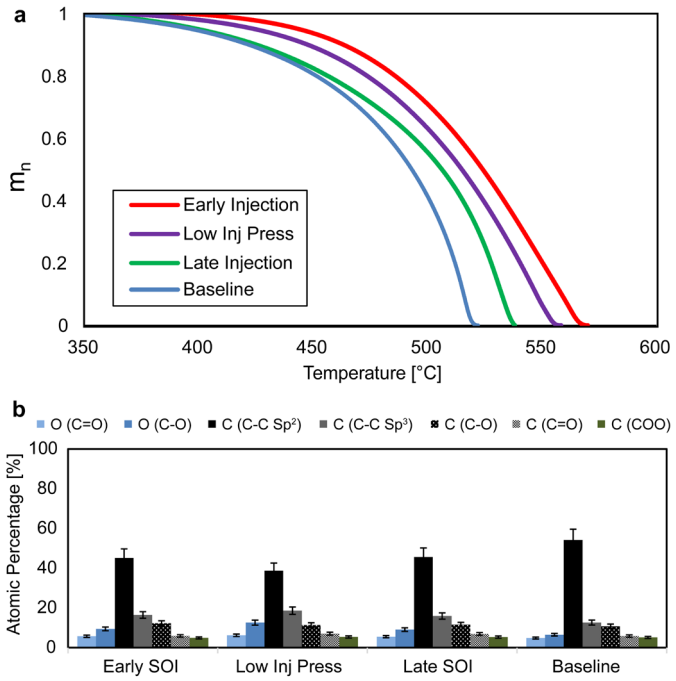


Figure 5. TG (a) and XPS (b) results for various particulate samples with respect to injection parameters (Early injection: SOI = 325 °CA bTDC, $P_{inj}$ = 6 MPa; Low injection pressure: SOI = 287 °CA bTDC, $P_{inj}$ = 2 MPa;, Late injection: SOI = 150 °CA bTDC, $P_{inj}$ = 6 MPa;, Baseline: SOI = 287 °CA bTDC, $P_{inj}$ = 6 MPa) (adapted from Ref. [99]).

As observed using SEM and TEM, Potenza, et al. [102] pointed out that when the rail pressure increased from 50 bar to 120 bar, the particulate cluster morphology changed from simple nanoparticle chains to nano-belts with core-shell structures, nanotubes and textured nanofoils. As reported by Kim, et al. [51], the radius of gyration and primary particle diameter for soot collected at $P_{inj.}$ = 150 bar were 50.10 ± 2.10 and 22.22 ± 0.22 nm, respectively, which are lower than 55.80 ± 3.07 and 22.53 ± 0.24 nm for soot generated at $P_{inj.}$ = 50 bar. This suggests that the higher injection pressure produced reduced soot agglomerates with smaller primary particles because of the improved soot oxidation. Extracted from HRTEM images, $L$ = 0.517 ± 0.046 nm and $T_f$ = 1.321 ± 0.012 of $P_{inj.}$ = 87.5 bar soot are similar to the values for $P_{inj.}$ = 100 bar soot [98]. However, there is a significant difference regarding the fringe separation distance for the above soot samples. For example, $D_s$ of $P_{inj.}$ = 87.5 bar soot was 0.405 ± 0.042 nm, which is significantly lower than that of $P_{inj.}$ = 100 bar soot (i.e. 1.187 ± 0.042 nm) [98]. Similarly, in the study by Kim, et al. [51], exhaust soot that was emitted by $P_{inj.}$ = 50 bar had a

lower fringe separation distance than that produced by $P_{inj.}$ = 150 bar. However, the discrepancies regarding the fringe separation distance between both samples were relatively smaller. These results indicate that increasing injection pressure results in a more disordered soot nanostructure.

Additionally, changes in the injection pressure influence PM composition. SEM-EDX shows that low injection pressure soot only presents carbon clusters, whereas high injection pressure soot exhibits traces of metallic polycrystalline agglomerates regarding the piston wear phenomenon [102]. When the injection pressure increased from 150 bar to 200 bar, the EC ratio tended to decrease, while the OC ratio increased [103]. Both vapor-phase and particulate-phase PAH concentrations gradually reduced when the injection pressure increased. However, when the injection pressure achieved 80 bar, the decline in the PAH concentration became less obvious [37]. The differences in oxygen-containing SFGs between different injection pressures are small, as presented in Figure 6 (b) [99]. In addition to the above discussions, there are limited studies on the effect of injection pressure on aliphatic C-H SFGs. As the injection pressure increased, a lower total PN concentration with a smaller geometric mean diameter was observed [104, 105]. As particulates with smaller mean diameters have a more available surface area for the adsorption of toxic compounds, more studies on the chemical properties of particulates produced by higher injection pressures are required.

### *3.4 Fuel injection timing*

Generally, early injection during the intake stroke is beneficial to homogenous fuel/air mixture formation. However, fuel that is injected too early (close to the top dead centre of the intake stroke) may cause fuel impingement on combustion chamber surfaces, which is the main source of pool fires. This causes high PM emissions [105, 106]. As fuel injection timing shifts from during the intake stroke to during the compression stroke, the time for air-fuel mixing becomes insufficient, thereby increasing the PM emissions. In addition, for wall-guided injection systems, the fuel spray may impinge on the cylinder walls and form a fuel film and more wall wetting. The injection timing determines not only the time available for pool

488 evaporation but also the amount of fuel impinging on the piston or the cylinder walls [107]. As
489 discussed earlier, injection timing significantly influences soot formation and oxidation, and
490 further affects soot oxidation reactivity and related features.

491 Koch, et al. [98] investigated the effect of injection timing on soot oxidation reactivity by
492 varying the start of injection (SOI) from 340 °CA to 220 °CA bTDC at the step of 30 °CA. The
493 results showed that the lowest $T_{max}$ of 520 ºC (i.e. the highest oxidation reactivity) was achieved
494 for the SOI of 310 °CA bTDC, which was related to the smallest soot particles that were
495 obtained by an engine exhaust particle sizer (EEPS) under this condition. Easter, et al. [108]
496 compared the oxidation reactivity of soot particles that were produced at three injection timings,
497 namely 325 °CA, 287 °CA and 150 °CA bTDC, respectively. Figure 6 (a) shows the TG results,
498 which indicate that soot reactivity from high to low can be ordered as follows: baseline
499 (287 °CA) > retarded SOI (150 °CA) > advanced SOI (325 °CA). Furthermore, the authors
500 found that the trend in soot reactivity agrees with the ash content. The above results of sweeping
501 SOI consistently showed that a SOI that leads to the highest soot reactivity and advanced or
502 retarded injection may reduce the reactivity.

503 Morphological observation showed that GDI soot that was generated at various injecting
504 timings presented a typical chain-like agglomerate structure, which was similar to diesel
505 agglomerates [81, 109]. The TEM analysis showed that both the agglomerated gyration radius
506 and the primary particle diameter decreased as the injection timing retarded. This result is in
507 agreement with the observation of Seong, et al. [81], who set a wider injection parameter from
508 330 °CA to 190 °CA bTDC. In addition, the authors claimed that the influence of injection
509 timing on the fractal dimension was insignificant. Barone, et al. [110] found that compared to
510 the optimised SOI of 280 °CA bTDC (regarding low PN concentrations), early fuel injections
511 (320 °CA bTDC) produced more particles with a larger primary particle diameter, which was
512 attributed to the increased fuel-rich zones in the cylinder. The consistent result that was obtained
513 from the TEM images that the primary particle size decreases along with the retarded injection
514 timing was confirmed in Ref. [111] through ultra-SAXS.

The effect of injection timing on soot nanostructure is more complicated, and the results vary. Easter [99] identified using both the Raman parameter of the D1/G peaks and visual observation of TEM images that varying the SOI had a negligible effect on soot nanostructure. This observation was further confirmed by quantitative analysis in Ref. [112], which reported that advanced injection timing from 303 °CA to 335 °CA bTDC had a negligible effect on both fringe length and tortuosity. However, although other scholars manifest that the injection timing may influence the soot nanostructure, their results are inconsistent. According to Koch, et al. [98], although soot particles with a SOI of 310 °CA bTDC exhibited a lower fringe length and separation distance, they showed a comparable fringe tortuosity than that of a SOI of 220 °CA bTDC. They concluded that a later injection resulted in poor homogenisation of the air/fuel mixture, which increased the graphene layer. This was further related to higher soot reactivity. Pan [113] found that regarding the retarded injection timing from 320 °CA to 240 °CA bTDC, the fringe tortuosity decreased, and the separation distance increased. Note that the variations in fringe tortuosity and separation distance may conflict, as reduced fringe tortuosity is usually accomplished by decreasing the separation distance and creating a more graphited arrangement of carbon layers [114]. Considering this, the author further confirmed using EELS that retarded injection timing led to a more ordered nanostructure. On the contrary, Kim, et al. [50] pointed out that an early injection with piston top wetting (320 °CA bTDC) had a smaller fringe separation distance than a late injection with liner wetting (180 °CA bTDC), which reveals that retarded injection timing causes a less-ordered structure. When the injection timing was retarded from 280 °CA to 220 °CA bTDC, Gaddam, et al. [84] reported that the fringe length decreased from 0.82 nm to 0.74 nm, whereas the fringe tortuosity slightly increased from 1.175 to 1.190. The contradictory findings from various researchers could be explained by the different engine configurations (i.e. injector position and wall-guided/spray-guided) and fuel properties (such as aromatic content and research octane number).

Unlike the above morphological analysis, investigations into the impact of SOI on soot chemical features were limited. Easter [99] found that the VOF increased with the retarded injection timing, and the differences between SOIs of 287 °CA and 150 °CA aTDC were small.

When obtained using the XPS, both early and late injection timings had a higher $sp^3/sp^2$ ratio. However, the oxygen-containing SFGs, including C-O, C=O and O-C=O, were similar among samples with three SOIs, as seen in Figure 6 (b) [99, 108]. In addition, Pan [113] reported that PAHs with four, five and six rings generally increased with the retarded injection timing.

### *3.5 EGR*

EGR is a common technique that is used to control $NO_x$ emissions in GDI engines. At part load, EGR acts as a diluent in unburnt gas, thus decreasing the peak in-cylinder temperature and $NO_x$ formation rates. The introduction of EGR could also change the PM features. Bogarra et al. [115, 116] examined the oxidation reactivity of soot samples collected from non-EGR and EGR with a rate of 19%, respectively. DTG curves showed that EGR soot exhibited a lower oxidation temperature than non-EGR soot. However, the authors found that the difference in the oxidation temperature between the two samples may be due to the different mass availability of soot rather than the variations in particle structure. According to the result of calculated activation energy, both samples showed similar values of approximately 100 kJ/mol, which confirmed the authors' speculation [115, 116].

From the morphology perspective, applying EGR reduced the primary particles' size and gyration radius. The reduced primary particle size may be attributed to the EGR capability of inhibiting soot nucleation, which overcomes the decreasing effect of post-flame oxidation caused by the lower temperature [117, 118]. The discrepancies in both the fractal dimension and number of primary particles per agglomerate were small, with or without EGR [117]. With a speed of 2000 r/min and the indicated mean effective pressure (IMEP) of 3 bar, applying EGR from 3.3% to 18% increased both the fringe tortuosity and separation distance. However, it had a negligible effect on fringe length, which indicates a more amorphous nanostructure [113]. Previously, Al-Qurashi, et al. [119] deconvoluted the chemical, dilution or thermal effects of EGR on the diesel soot features. Considering the different soot formation mechanisms regarding applying EGR for diesel and GDI engines, more fundamental research is required to quantify the weight of these three effects on the variations in the morphology and nanostructure

of GDI soot. Figure 8 presents the effect of the EGR with a ratio of 19% on fringe parameters under different SOIs, according to the data in Ref. [112]. Interestingly, EGR slightly increased the fringe length and interlayer spacing, but no significant trends in tortuosity were observed. The authors further concluded that adopting 19% EGR had a negligible influence on soot nanostructure [112]. In diesel engines, the impact of EGR on soot nanostructure and oxidation is related to the operating point [120, 121]. In this regard, more work is required to clarify the reasons behind these different trends.

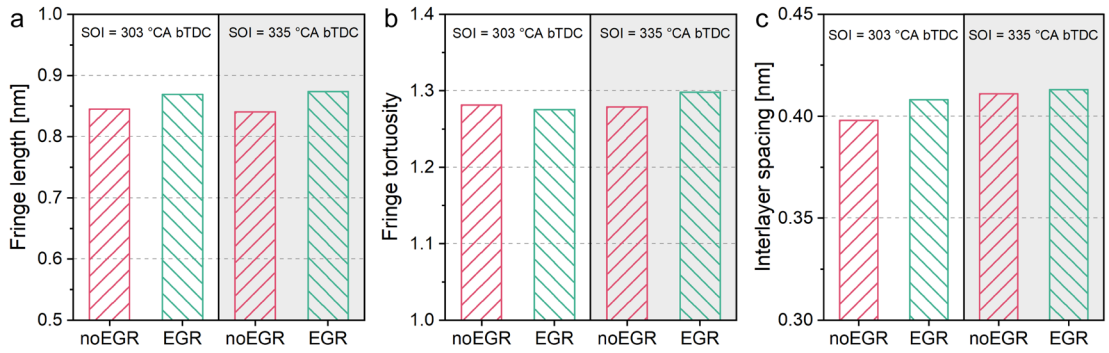


Figure 6. Effect of EGR on fringe parameters under different SOIs: (a) fringe length, (b) fringe tortuosity, and (c) interlay spacing (data from Ref. [112]).

The influence of EGR on PAH concentrations is dependent on engine operating conditions, according to various researchers [37, 113]. At 2000 r/min and IMEP = 7.5 bar, An, et al. [37] found that applying EGR with a lower ratio (i.e. 2.5%) significantly reduced the particulate-phase PAH concentration, compared with the non-EGR condition. With the further increase of the EGR ratio, a negligible change in the particulate-phase PAH concentration was observed. However, in Ref. [113], at 2000 r/min and IMEP = 3 bar, increasing the EGR ratio from 0% to 18% gradually increased the particulate-phase PAH concentrations. As particulate-phase PAHs with five or six rings were predominantly absorbed on soot cores [37], it may verify the assumption that the impact of EGR on soot nanostructure and oxidation in GDI engines is related to the operating point.

In addition to the operating parameters that are discussed above, PM emissions from GDI engines are influenced by other factors, such as spark timing, intake boost, multiple injections

and injector deposits. However, there are limited studies on the impact of these factors on PM features. Therefore, further research on the effects of these factors is necessary to better reveal the control strategy of particulate aftertreatments of GDI engines.

# 4 Influences of exhaust aftertreatment technologies on soot features

Exhaust aftertreatments, such as TWC and GPF, are essential to control both gaseous and particulate pollutants to meet the increasingly stringent emission regulations. Amongst them, TWCs have been widely used for decades due to their effective removal of HC, CO and $NO_x$ emissions. It should be noted that the impact of TWCs on soot particles is not negligible although they are not specifically designed to reduce particle emissions in the exhaust [122]. As HC emissions are important components of semi-volatile particles, TWCs can remove the precursors of semi-volatile components and significantly reduce the exhaust particulate mass and number [123]. In addition, the high temperature and the presence of catalysts in the TWC may influence the soot features. As mentioned earlier, TWCs greatly affect PM emissions as GPFs are designed to trap the exhaust particles. A previous study on diesel soot suggested that understanding the changes in soot features along the aftertreatments contributes to the optimisation of soot elimination [124]. Therefore, the effects of TWC and GPF on soot features are summarised below.

## *4.1 TWC*

Bogarra, et al. [112] observed that the TWC had no significant effect on soot reactivity, as the residence time of PM in the TWC is too limited. However, Choi, et al. [63] stated that PM that was collected from the TWC downstream showed higher soot oxidation reactivity than that generated from the TWC upstream. This is attributed to the higher ash content in PM after TWC, which provides the catalytic effect on soot oxidation.

Endo, et al. [90] found that a reduction in the mean primary particle diameter from 17.6 nm before TWC to 15.0 nm after TWC was observed under the operating condition. The PM is primarily composed of dry soot, which is covered by a soluble organic fraction (SOF). When the exhaust flow passes through, larger particles are collected on the coat in the TWC, and some

SOFs become oxidised due to the presence of the catalyst. This can be testified in Ref. [63], where it was reported that under the given operating conditions, TWC reduced VOF from 5.14% to 2.02% due to the oxidation of organic components. Therefore, the use of TWC decreases the size of the primaries. Regarding the soot nanostructure, Bogarra, et al. [112] pointed out that the fringe parameters exhibited no significant changes before and after TWC. The authors speculated that the soot may be deposited in the TWC by diffusion rather than be oxidised. However, numerous studies show that due to the presence of the catalyst, soot is oxidised easier [125-127]. Such a change in the soot oxidation process may change the soot structure. It can be hypothesised that a relatively higher exhaust temperature with the presence of a catalyst in the TWC could influence the soot features. Therefore, more studies are required to clarify the effect of TWC on soot reactivity and its related features.

### *4.2 GPF*

Liu, et al. [128] pointed out that by combining thermophoretic sampling with TEM observations, the use of GPF has a negligible effect on the visual morphology of soot agglomerates. However, as expected, the number of primary particles in a certain TEM image significantly reduces after GPF. Moreover, the $D_f$ of agglomerates after GPF was lower than that of before GPF, which indicates that the agglomerates after GPF present a more branched and less compact structure [128]. According to Endo, et al. [90], the mean radii of the gyration of agglomerates before and after GPF were 56.5 nm and 82.0 nm, respectively. The significant increase in agglomerate size after GPF could be because particles are easily collected in the GPF [90]. However, the trends in the morphological parameters of particulates from a GDI vehicle during transient drive cycles are different from the above results from the steady-state engine tests. Saffaripour, et al. [129] performed a comparative study on the effect of GPF on the size and morphology of particulates from a GDI vehicle over the Federal Test Procedure (FTP-75) and the US06 Supplemental Federal Test Procedure (US06) transient drive cycles. Their results showed that the fractal dimension of soot aggregates was not affected by GPF. Moreover, over the whole range of driving cycles, particulates from the vehicle without GPF presented slightly higher agglomerates but smaller primary particle sizes than those collected

from the GPF-equipped vehicle.

Extracted from HRTEM images, soot collected from the GPF downstream showed a smaller mean fringe length, fringe tortuosity and interlayer spacing than the sample from the GPF upstream [128]. Soot with a more ordered structure generally presents a longer fringe length and smaller tortuosity and interlayer spacing. Based on the results reported in Ref. [128], it is difficult to quantify and classify whether the reduced fringe length or smaller tortuosity and interlay spacing is governing the trends in soot nanostructure. Therefore, a supplementary analysis using Raman spectrometer or/and XRD could be conducted to assess the variations in soot nanostructure between the GPF upstream and downstream.

As reported in Ref. [130], the application of GPF significantly reduces the emissions of particulate- and vapor-phase PAHs. Moreover, for various GDI vehicles over the LA92 cycle, employing GPF reduced the particulate- and vapor-phase PAHs by 98% and 57.5% on average, respectively. A similar phenomenon was observed by Munoz, et al. [131], who pointed out that the effects of GPF on removing semi-volatile compounds were not as strong as for solid particles. This is attributed to the volatility of the semi-volatile PAHs, which enables them to escape from the soot-loaded filter at higher temperatures. Having compared four types of GPFs, it is uncertain whether GPFs with coated catalysts could remove PAHs. However, GPFs exhibited higher filtration efficiencies in PAHs over the cold WLTC than over the hot WLTC [131].

In modern GDI engines, both TWC and GPF are the indispensable exhaust aftertreatments that meet the Euro VI or future emission regulations. The above discussions show that although some research has been conducted on the effect of TWC or GPF on the soot features, the results are often contradictory. In addition, studies that focus on variations of soot oxidation reactivity and related features, such as morphology, nanostructure and chemical components, in the entire exhaust path of GDI engines are limited. In this regard, investigations into the variations in GDI soot features along the exhaust aftertreatments, including before TWC, after TWC (i.e. before GPF), after GPF and inside the GPF, are encouraged. It can be speculated that soot inside the

GPF has a higher oxidation reactivity than soot collected the GPF upstream. Figure 7 displays the interactions of soot and ash particles during the soot oxidation processes [63]. As stated by Choi, et al. [63], ash particles, particularly the combustion-derived ash precursor significantly promotes soot oxidation due to the catalytic effect. With the accumulation of soot particles in the filter, ash fraction increases, and thus the promoting effect on soot oxidation may be more apparent.

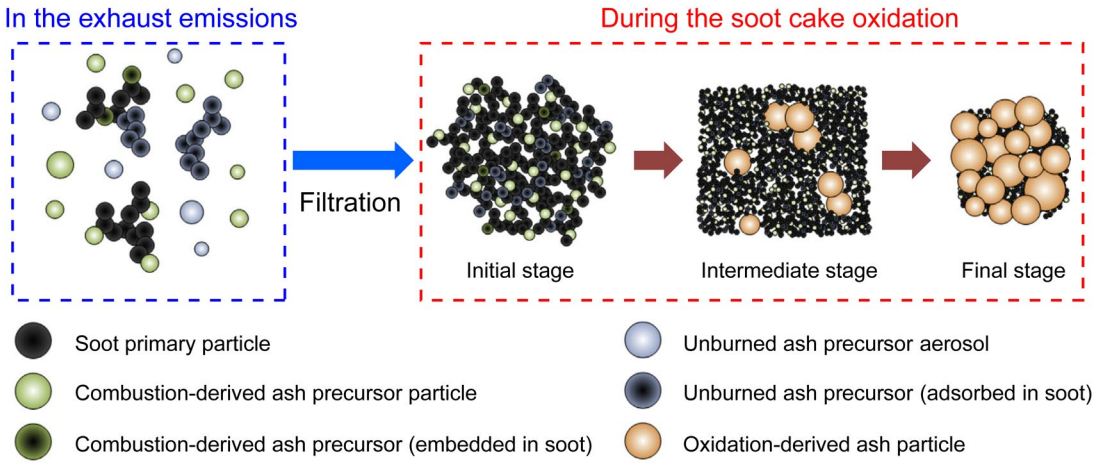


Figure 7. Conceptual drawings of the interactions of soot and ash particles during the soot oxidation processes (adapted from Ref. [63]).

## 3 The features of soot particles from oxygenated fuels

Fuel reformulation changes the physical and chemical features of the fuel and influences the air-fuel mixing process and soot-forming combustion reaction pathways [132, 133]. From the soot formation perspective, the coalescence during the combustion of unsaturated hydrocarbon (especially the PAHs) initiates soot formation. Mixing with oxygenates dilutes the content of unsaturated hydrocarbon in the fuel, which benefits the inhibition of nascent soot formation. Another effect of oxygenated fuel combustion is the promotion of soot oxidation. However, in practical GDI engines, blending with oxygenated fuels may affect fuel injection and spray due to the modified vapor pressure, heating value and enthalpy of vaporisation. As these factors may compete, it remains inconclusive regarding whether mixing with oxygenated fuels causes an increase or decrease in PM mass and PN emissions from current GDI engines [44, 45]. Here, we discuss the effect of mixing with oxygenated fuels on soot features. Ethanol

695 is the most popular additive amongst the oxygenates used in GDI engines due to its high octane
696 number, oxygen content and latent heat of vaporisation [134]. In addition to the ethanol, other
697 oxygenated additives, such as methanol, n-butanol, 2,5-dimethylfuran (DMF) and dimethyl
698 carbonate (DMC), are used in GDI engines. However, their impacts on soot features have rarely
699 been evaluated, as the available literature has mainly focused on the variations in soot
700 morphological structures with the addition of these additives. Table 3 lists the summary of
701 physicochemical features of soot particles from oxygenated fuels.

702 The soot samples from gasoline-ethanol blends exhibited lower activation energies and
703 higher oxidation reactivity, which was independent of the combustion systems (air-guided or
704 wall-guided), ethanol content and operating points [39, 83]. Figure 10 presents the
705 thermogravimetric curves of particulate samples emitted from gasoline fuel and
706 gasoline/ethanol blends. With the increase of ethanol concentration from 10% to 20%,
707 oxidation temperatures (defined as the temperatures at which the maximum thermogravimetric
708 rate in Figure 10) of soot samples gradually decreased, indicating a growing trend towards
709 oxidation [39]. The activation energy of pure ethanol-derived soot was the lowest at 83 kJ/mol,
710 followed by DMF-derived soot (109 kJ/mol), E25 (25 vol% ethanol + 75 vol% gasoline)-
711 derived soot (124 kJ/mol) and gasoline-derived soot (153 kJ/mol) [83]. This is consistent with
712 the result of Guerrero Peña, et al. [135], who claimed that the diffusion flame soot of E20 (20
713 vol% ethanol + 80 vol% gasoline) was the most reactive, whereas the reactivity of soot
714 generated from gasoline was the least. Regarding DMF20 (20 vol% DMF + 80 vol% gasoline)
715 soot, the oxidation reactivity is between that of gasoline and E20. In their study, the highest
716 reactivity of E20 soot was attributed to it having the highest oxygen and hydrogen content via
717 elemental analysis, an amorphous nanostructure characterised by HRTEM, EELS and XRD and
718 the highest concentrations of oxygenated and aliphatic functional groups on its surface, as
719 examined by FTIR [135]. Moreover, soot collected from DMC8 (8 vol% DMC + 92 vol%
720 commercial gasoline) displayed a lower starting and maximum oxidation temperature than soot
721 generated from commercial gasoline, which indicates higher oxidation reactivity [136].
722 Similarly, for most diesel engines, the combustion of oxygenated fuels tends to emit soot with

higher oxidation reactivity [88, 137, 138].

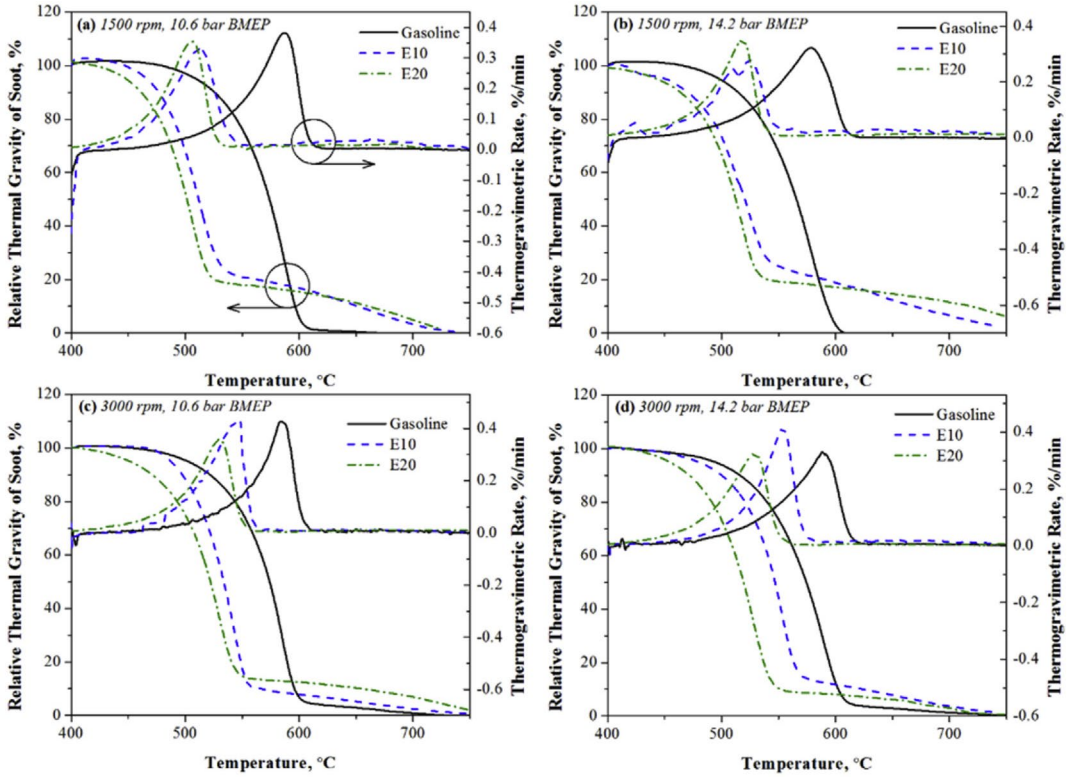


Figure 8. Thermogravimetric curves of particulate samples emitted from gasoline fuel and gasoline/ethanol blends (adapted from Ref.[39]).

Particulates from gasoline mixing with oxygenated fuels display spherical chain-like or cluster-like agglomerates and show no significant visual differences in micro-scale morphology amongst most PM samples. However, regarding E25 soot in Ref. [139], the TEM images of the particles showed the coexistence of fractal-like agglomerates and some small HC droplets. According to the TEM images, mixing with ethanol and DMC generally decreases the agglomerate and primary particle sizes [52, 136, 139]. The presence of oxygen and the absence of aromatics reduce the average number of primary particles per agglomerate, which results in a smaller agglomerate size. As is widely accepted, the primary particle size results from the competition of surface growth and soot oxidation. From a fuel component perspective, both the dilution and oxygen effects of the addition of oxygenated fuels not only suppress the soot surface growth but also promote soot oxidation. This is in agreement with the soot luminosity images that were observed by Gao, et al. [52], which show that mixtures with higher ethanol

739 contents significantly reduced the pool fires and soot formation, despite possibly higher wall
740 wetting caused by a larger injection duration and higher density and viscosity. It is interesting
741 to note that the soot morphology between gasoline and B33 (33 vol% butanol +67 vol%
742 gasoline) is relatively slight, as reported by Hergueta, et al. [139]. This may be attributed to the
743 consequence of the fuel spray patterns and combustion conditions. Another explanation is the
744 coagulation mechanism related to the higher combustion temperatures of B33 combustion.
745 However, Sharma and Agarwal [85, 140] found that the impact of gasohols on the primary
746 particle size is connected to the engine load, as the $d_p$ reduced as the fuel oxygen content at the
747 part-load increased, whereas at full load, the $d_p$ increased as the fuel oxygen content increased.
748 Moreover, the authors stated that the soot agglomerates mainly presented chain-like structures,
749 and no significant difference was observed between gasoline and gasohols. However, Lee, et al.
750 [141] found that E20 yielded no statistically pronounced impact on the mean primary particle
751 diameter.

752 A visual inspection of the HRTEM images showed that primary particles emitted from
753 gasoline and its blends present the typical shell-core structure, i.e. graphene-like segments with
754 longer fringes at the outer shell region and PAH layers with chaotic orientations at the inner
755 core region [52, 136, 140]. However, the addition of oxygenated fuels changes the soot
756 nanostructure, as the combustion-related parameters, such as residence time, reaction
757 temperature and oxygen concentration, differ. Generally, adding oxygenates into gasoline
758 produces particles with a more amorphous structure, as shown by both HRTEM and RS [52,
759 136, 142]. When the ethanol concentrations increased from 0% to 60%, the fringe length almost
760 linearly reduced, along with the growth in both fringe tortuosity and separation distance, which
761 indicates a less graphitised structure [52]. The higher $A_{D1}/A_G$ (area ratio of D1 band to G band)
762 and $A_{D3}/A_G$ (area ratio of D3 band to G band) of DMC8 soot implied that it was smaller in
763 graphitic and higher in amorphous concentration [136]. This phenomenon may be due to the
764 lower in-cylinder temperature [136] and shorter soot residence time [52], which reduces the
765 graphitisation process of the graphene layers. However, as reported by Lee, et al. [141], the
766 impact of E20 on soot nanostructure is sensitive to injection timing. For example, at the SOI of

310 °CA bTDC, E20 soot showed a more amorphous structure than gasoline soot, whereas at the SOI of 250 °CA bTDC, the primary particles from both fuels exhibited graphitic structures.

Regarding the chemical components, mixing with ethanol and DMC increased the VOF content in PM [39, 136]. This may be because adding oxygenated fuels inhibits the formation of soot precursors and reduces the fraction of elemental soot in PM. As expected, Luo, et al. [39] found that E10 (10% ethanol + 90% gasoline, by vol.) decreased the concentration of most PAHs, except those with small aromatic rings, such as naphthalene. Similarly, with the increase of ethanol in gasoline from 10% to 83%, the elemental carbon fraction was markedly reduced [34]. Moreover, Sharma, et al. [85] reported that particulates from gasohols had relatively lower trace metal concentrations than that from gasoline.

From the publications available, mixing with oxygenated fuels increases the soot oxidation reactivity, which can benefit the regeneration of GPFs, as a lower energy input is required to oxidise the accumulated particles. Generally, oxygenated fuel-derived soot particles emitted smaller agglomerates with smaller primaries, which could cause the absence of soot cake and reduce filtration efficiency. Therefore, for the blended fuels, the design may need to be optimised by changing the filter material porosity or/and the filter wall size to achieve a balance between pressure drop and filtration efficiency. Moreover, soot produced from oxygenated fuels presents a less-ordered nanostructure. This seems to be highly linked to higher oxidation reactivity. It is worth noting that studies on the chemical properties of soot particulates from oxygenated fuels are limited. Further research is necessary to clarify the impact of adding oxygenated fuels on soot chemical features, such as surface functional groups.

788 Table 3. Summary of physicochemical features of soot particles from oxygenated fuels.

| References | Engine type | Test fuel | Analytic methods | Main results |
|---|---|---|---|---|
| Luo, et al. [39] | wall-guided, 2.0 L, 9.2:1 | Gasoline, E10, E20 | TGA, GC-MS | Ethanol enhances soot oxidation reactivity and increases VOF content.<br>Blended fuels reduce concentrations of most PAHs, except those with small aromatic rings. |
| Wang, et al. [83] | spray-guided, 0.565L, 11.5:1 | Gasoline, E25, DMF, E100 | TGA | Ranking of soot reactivity: E100 > DMF > E20 > Gasoline. |
| Lee, et al. [141] | -, 0.549 L, 11.97:1 | Gasoline, E20 | TEM | E20 has a negligible effect on the mean primary particle diameter.<br>At an SOI of 250 °CA bTDC, primary particles from both fuels exhibit graphitic structures, whereas at an SOI of 310 °CA bTDC, the E20 particle shows a more amorphous structure. |
| Gao, et al. [52] | wall-guided, 0.5 L, 10.5:1 | Gasoline, E10, E35, E60 | TEM | Increasing ethanol concentration decreases the sizes of agglomerates and primary particles, and stretches the agglomerate structures.<br>As the ethanol ratio increases, more amorphous nanostructures are observed. |
| Sharma, et al. [85] | wall-guided, 0.5 L, 10.5:1 | Gasoline, E15, M15 | TEM, STEM-EDS | At part load, $d_p$ reduces as the fuel oxygen content increases.<br>At full load, $d_p$ increases as the fuel oxygen content increases.<br>Insignificant difference in agglomerates was observed between the particles from various test fuels.<br>The concentration of trace metals is lower in E15 than gasoline and M15. |
| Hergueta, et al. [139] | air-guided, 2.0 L, 10:1 | Gasoline, E25, B33 | TEM | E25 soot exhibits the smallest and the most chain-like agglomerates with the smallest primary particle size.<br>Gasoline soot presents the largest and the most compact agglomerates with the largest primary particle size.<br>The difference in soot morphology between gasoline and B33 is relatively small. |
| Sharma, et al. [142] | wall-guided, 0.5 L, 10.5:1 | Gasoline, E15, B15, M15 | ICP-OES, RS, FTIR, HRTEM | Particulates from gasohols exhibit a more amorphous structure than those from gasoline.<br>Particulates from gasohols have lower trace metal concentrations than those from gasoline. |

| | | | | |
|---|---|---|---|---|
| Sharma, et al. [140] | wall-guided, 0.5 L, 10.5:1 | Gasoline, B15 | TEM | Compared to gasoline, B15 soot exhibits a smaller $d_p$ at partial load and a larger $d_p$ at full load. Soot agglomerates present chain-like structures, and there is insignificant difference between both fuels. |
| Karavalakis, et al. [34] | wall-guided, 5.3 L, - | E10, E51, E83, iBu55 | TOC | Increasing ethanol content reduces the EC fraction significantly. Regarding iBu55, the EC concentration is almost the same as the OC fraction. |
| Chan, et al. [136] | air-guided, 2.0 L, 10:1 | Gasoline, DMC8 | TGA, TEM, RS | DMC8 soot has a larger proportion of VOF and a higher oxidation reactivity. DMC8 soot shows smaller primary particle and agglomerates sizes than gasoline soot and a more disordered structure. |

789

# 5 Conclusions and outlook

GDI particulates have become an emerging environmental concern with the penetration of GDI engine-powered vehicles in recent years. GPFs are essential for GDI engines to meet the increasingly stringent particulate regulations. A better understanding of PM characteristics is crucial to develop smart GPF management systems and extend the catalyst's life of GPF. In addition, the physical and chemical characteristics of soot particles can provide useful information on PM formation and the assessment of exhaust toxicity and environmental impacts. Therefore, this review attempted to comprehensively describe the physicochemical features of soot particulates from GDI engines.

In-flame soot samples collected on the exhaust valve side or generated from the piston-wetting condition have a longer residence time and exhibit a more carbonised structure. However, compared to in-flame soot, GDI exhaust soot presents a more stable and graphitic nanostructure, which makes it harder to oxidise. In addition to carbonaceous soot, ash particles, which are mainly originated from the in-cylinder consumed lubricating oil, are observed in GDI exhaust particulate samples. Accordingly, in addition to the main components (e.g. C and O), element components including Ca, P, Na, Si and Zn are detected in soot particles from GDI vehicles. Compared to diesel exhaust particles, GDI soot contains more inorganic and metallic elements. Additionally, GDI soot is usually smaller, less ordered and more reactive than diesel soot. However, further researches are needed to present a complete picture of soot features from in-cylinder to the atmosphere, including: i) revealing instantaneous features of in-cylinder soot as a function of crank angle degrees; and ii) clarifying the differences in soot features from the exhaust valve into the atmosphere.

The effects of engine operating parameters (i.e. engine speed and load, equivalence ratio, fuel injection pressure and timing, and EGR) and aftertreatments (i.e. TWC and GPF) are systematically discussed. However, no consensus has been reached which could be attributed to the complexity of analytic techniques, the variations in engine specifications and fuel properties, and the heterogeneity of soot samples. The effects of engine speed and load on GDI

soot features are smaller than on diesel soot. Higher injection pressures promote soot oxidation, and there is an optimal SOI to enhance soot oxidation reactivity. Both EGR and TWC have a minor effect on soot reactivity. Although GPF significantly reduces PAH emissions, it has a minor effect on soot morphology. Future studies need to evaluate more influencing factors, such as spark timing, intake boost, multiple injections and injector deposits.

Mixing with oxygenated fuels enhances the soot oxidation reactivity and benefits the regeneration of GPFs. In addition, oxygenated fuel-derived soot particles have smaller agglomerates with smaller primaries, which implies that the design of the filter material porosity and wall size must be optimised to maintain the filtration efficiency. Regarding the fuel components and properties, more work is required to investigate the effect of the physical and chemical properties of gasoline fuel on soot features.

## Acknowledgements

This work was supported by the National Natural Science Foundation of China (52006014, 52106191), the China Postdoctoral Science Foundation (2020M683396, 2021T140584), the Innovation Capability Support Program of Shaanxi (Program No. 2021TD-28), the Youth Innovation Team of Shaanxi Universities, the Fundamental Research Funds for the Central Universities, CHD (300102222104, 300102222509), and Beijing Institute of Technology Research Fund Program for Young Scholars (XSQD-202203001). The fourth author Y.H. is a recipient of the ARC Discovery Early Career Research Award (DE220100552).

## References

[1] C. Liu, R. Chen, F. Sera, A.M. Vicedo-Cabrera, Y. Guo, S. Tong, M.S.Z.S. Coelho, Ambient Particulate Air Pollution and Daily Mortality in 652 Cities, The New England Journal of Medicine 381 (2019) 705-715.

[2] S. Weichenthal, T. Olaniyan, T. Christidis, E. Lavigne, Marianne, Hatzopoulou, K.V. Ryswyk, M. Tjepkema, R. Burnett, Within-city Spatial Variations in Ambient Ultrafine Particle Concentrations and Incident Brain Tumors in Adults, Epidemiology 31(2) (2020) 177-183.

[3] A. Joshi, Review of Vehicle Engine Efficiency and Emissions, SAE Technical Paper 2019-01-0314, 2019.
[4] A. Überall, R. Otte, P. Eilts, J. Krahl, A literature research about particle emissions from engines with direct gasoline injection and the potential to reduce these emissions, Fuel 147 (2015) 203-207.
[5] H. Chong, S.Y. Yang, K.O. Lee, Accurate Measurements of Heat Release, Oxidation Rates, and Soluble Organic Compounds of Diesel Particulates through Thermal Reactions, SAE Technical Paper 2010-01-0814, 2010.
[6] M. Lapuerta, J. Rodríguez–Fernández, J. Sánchez-Valdepeñas, Soot reactivity analysis and implications on diesel filter regeneration, Prog. Energy Combust. Sci. 78 (2020) 100833.
[7] Y. Guo, Z. Ristovski, E. Graham, S. Stevanovic, P. Verma, M. Jafari, B. Miljevic, R. Brown, The correlation between diesel soot chemical structure and reactivity, Carbon 161 (2020) 736-749.
[8] H. Al Housseiny, M. Singh, S. Emile, M. Nicoleau, R.L. Vander Wal, P. Silveyra, Identification of Toxicity Parameters Associated with Combustion Produced Soot Surface Chemistry and Particle Structure by in Vitro Assays, Biomedicines 8(9) (2020) 345.
[9] H.S. Kwon, M.H. Ryu, C. Carlsten, Ultrafine particles: unique physicochemical properties relevant to health and disease, Experimental & Molecular Medicine 52(3) (2020) 318-328.
[10] S. Arias, F. Molina, J.R. Agudelo, Palm oil biodiesel: An assessment of PAH emissions, oxidative potential and ecotoxicity of particulate matter, Journal of Environmental Sciences 101 (2021) 326-338.
[11] X. Wang, Y. Wang, Y. Bai, P. Wang, Y. Zhao, An overview of physical and chemical features of diesel exhaust particles, Journal of the Energy Institute 92(6) (2019) 1864-1888.
[12] M.A. Ghadikolaei, P.K. Wong, C.S. Cheung, Z. Ning, K.-F. Yung, J. Zhao, N.K. Gali, A.V. Berenjestanaki, Impact of lower and higher alcohols on the physicochemical properties of particulate matter from diesel engines: A review, Renewable and Sustainable Energy Reviews 143 (2021) 110970.
[13] J.A. Soriano, J.R. Agudelo, A.F. López, O. Armas, Oxidation reactivity and nanostructural characterization of the soot coming from farnesane - A novel diesel fuel derived from sugar cane, Carbon 125 (2017) 516-529.
[14] D. Mao, M.A. Ghadikolaei, C.S. Cheung, Z. Shen, W. Cui, P.K. Wong, Influence of alternative fuels on the particulate matter micro and nano-structures, volatility and oxidation reactivity in a compression ignition engine, Renewable and Sustainable Energy Reviews 132 (2020) 110108.
[15] B. Wang, Y.-S. Lau, Y. Huang, B. Organ, H.-C. Chuang, S.S.H. Ho, L. Qu, S.-C. Lee, K.-F. Ho, Chemical and toxicological characterization of particulate emissions from diesel vehicles, Journal of Hazardous Materials 405 (2021) 124613.
[16] C.D. Ávila, M.L. Botero, A.F. Agudelo, J.R. Agudelo, An assessment on how different collection methods impact thermal properties, surface functional groups, nanostructure and morphology of diesel particulate matter, Combustion and Flame 225 (2021) 74-85.
[17] X. Wang, Y. Wang, Y. Bai, Q. Duan, Properties and oxidation of exhaust particulates from dual fuel combustion: A comparative study of premixed gasoline, n-butanol and their blends, Environmental Pollution 271 (2021) 116391.
[18] X. Wang, Y. Wang, Y. Bai, F. Guo, D. Wang, Oxidation and nanostructural characterization of exhaust particulates from gasoline/diesel dual-fuel combustion, Fuel 298 (2021) 120837.
[19] J. Gao, H. Chen, J. Chen, C. Ma, G. Tian, Y. Li, Explorations on the continuous oxidation kinetics of diesel PM from heavy-duty vehicles using a single ramp rate method, Fuel 248 (2019) 254-257.
[20] J. Gao, C. Ma, S. Xing, L. Sun, Oxidation behaviours of particulate matter emitted by a diesel engine equipped with a NTP device, Applied Thermal Engineering 119 (2017) 593-602.
[21] X. Wang, Y. Wang, F. Guo, D. Wang, Y. Bai, Physicochemical characteristics of particulate matter emitted by

886 diesel blending with various aromatics, Fuel 275 (2020) 117928.
887 [22] K.O. Lee, R. Cole, R. Sekar, M.Y. Choi, J.S. Kang, C. Bae, H.D. Shin, Morphological investigation of the
888 Microstructure Dimensions, and Fractal Geometry of Diesel particulates, P. Combust. Inst. 29 (2002) 647–653.
889 [23] K.O. Lee, J. Zhu, S. Ciatti, Sizes, Graphitic Structures and Fractal Geometry of Light-Duty Diesel Engine
890 Particulates, SAE Technical Paper 2003-01-3169, 2003.
891 [24] R.L. Vander Wal, A.J. Tomasek, M.I. Pamphlet, C.D. Taylor, W.K. Thompson, Analysis of HRTEM images
892 for carbon nanostructure quantification, J. Nanopart. Res. 6(6) (2005) 555-568.
893 [25] K. Yehliu, R.L. Vander Wal, A.L. Boehman, Development of an HRTEM image analysis method to quantify
894 carbon nanostructure, Combust. Flame 158(9) (2011) 1837-1851.
895 [26] M.L. Botero, Y. Sheng, J. Akroyd, J. Martin, J.A.H. Dreyer, W. Yang, M. Kraft, Internal structure of soot
896 particles in a diffusion flame, Carbon 141 (2019) 635-642.
897 [27] B. Rohani, C. Bae, Effect of exhaust gas recirculation (EGR) and multiple injections on diesel soot nano-
898 structure and reactivity, Appl. Therm. Eng. 116 (2017) 160-169.
899 [28] G.D.J. Guerrero Peña, A. Raj, S. Stephen, T. Anjana, Y.A.S. Hammid, J.L. Brito, A.A. Shoaibi,
900 Physicochemical properties of soot generated from toluene diffusion flames: Effects of fuel flow rate, Combustion
901 and Flame 178 (2017) 286-296.
902 [29] J. Gao, C. Ma, F. Xia, S. Xing, L. Sun, L. Huang, Raman characteristics of PM emitted by a diesel engine
903 equipped with a NTP reactor, Fuel 185 (2016) 289-297.
904 [30] A. Sadezky, H. Muckenhuber, H. Grothe, R. Niessner, U. Pöschl, Raman microspectroscopy of soot and
905 related carbonaceous materials: Spectral analysis and structural information, Carbon 43(8) (2005) 1731-1742.
906 [31] A. Liati, D. Schreiber, Y. Arroyo Rojas Dasilva, P. Dimopoulos Eggenschwiler, Ultrafine particle emissions
907 from modern Gasoline and Diesel vehicles: An electron microscopic perspective, Environ Pollut 239 (2018) 661-
908 669.
909 [32] W. Mühlbauer, C. Zöllner, S. Lehmann, S. Lorenz, D. Brüggemann, Correlations between physicochemical
910 properties of emitted diesel particulate matter and its reactivity, Combust. Flame 167 (2016) 39-51.
911 [33] X. Li, Z. Xu, C. Guan, Z. Huang, Particle size distributions and OC, EC emissions from a diesel engine with
912 the application of in-cylinder emission control strategies, Fuel 121 (2014) 20-26.
913 [34] G. Karavalakis, D. Short, V. Chen, C. Espinoza, T. Berte, T. Durbin, A. Asa-Awuku, H. Jung, L. Ntziachristos,
914 S. Amanatidis, A. Bergmann, Evaluating Particulate Emissions from a Flexible Fuel Vehicle with Direct Injection
915 when Operated on Ethanol and Iso-butanol Blends, SAE Technical Paper 2014-01-2768, 2014.
916 [35] L. Wang, C. Song, J. Song, G. Lv, H. Pang, W. Zhang, Aliphatic C–H and oxygenated surface functional
917 groups of diesel in-cylinder soot: Characterizations and impact on soot oxidation behavior, P. Combust. Inst. 34(2)
918 (2013) 3099-3106.
919 [36] Y. Liu, C.L. Song, G. Lv, X.F. Cao, L. Wang, Y.H. Qiao, X.L. Yang, Surface functional groups and $sp^3/sp^2$
920 hybridization ratios of in-cylinder soot from a diesel engine fueled with n-heptane and n-heptane/toluene, Fuel 179
921 (2016) 108-113.
922 [37] Y.Z. An, S.P. Teng, Y.Q. Pei, J. Qin, X. Li, H. Zhao, An experimental study of polycyclic aromatic
923 hydrocarbons and soot emissions from a GDI engine fueled with commercial gasoline, Fuel 164 (2016) 160-171.
924 [38] M. Muñoz, R. Haag, P. Honegger, K. Zeyer, J. Mohn, P. Comte, J. Czerwinski, N.V. Heeb, Co-formation and
925 co-release of genotoxic PAHs, alkyl-PAHs and soot nanoparticles from gasoline direct injection vehicles,
926 Atmospheric Environment 178 (2018) 242-254.
927 [39] Y. Luo, L. Zhu, J. Fang, Z. Zhuang, C. Guan, C. Xia, X. Xie, Z. Huang, Size distribution, chemical

928 composition and oxidation reactivity of particulate matter from gasoline direct injection (GDI) engine fueled with
929 ethanol-gasoline fuel, Applied Thermal Engineering 89 (2015) 647-655.
930 [40] A. Baldelli, U. Trivanovic, T.A. Sipkens, S.N. Rogak, On determining soot maturity: A review of the role of
931 microscopy- and spectroscopy-based techniques, Chemosphere 252 (2020) 126532.
932 [41] S. Choi, C.L. Myung, S. Park, Review on characterization of nano-particle emissions and PM morphology
933 from internal combustion engines: Part 2, International Journal of Automotive Technology 15(2) (2014) 219−227.
934 [42] J. Wei, Y. Wang, Effects of biodiesels on the physicochemical properties and oxidative reactivity of diesel
935 particulates: A review, Science of the Total Environment 788 (2021) 147753.
936 [43] E.S. Galvao, J.M. Santos, A.T. Lima, N.C. Reis, Jr., M.T.D. Orlando, R.M. Stuetz, Trends in analytical
937 techniques applied to particulate matter characterization: A critical review of fundaments and applications,
938 Chemosphere 199 (2018) 546-568.
939 [44] Y. Qian, Z. Li, L. Yu, X. Wang, X. Lu, Review of the state-of-the-art of particulate matter emissions from
940 modern gasoline fueled engines, Applied Energy 238 (2019) 1269-1298.
941 [45] M. Raza, L. Chen, F. Leach, S. Ding, A Review of Particulate Number (PN) Emissions from Gasoline Direct
942 Injection (GDI) Engines and Their Control Techniques, Energies 11(6) (2018) 1417.
943 [46] O.I. Awad, X. Ma, M. Kamil, O.M. Ali, Z. Zhang, S. Shuai, Particulate emissions from gasoline direct
944 injection engines: A review of how current emission regulations are being met by automobile manufacturers,
945 Science of the Total Environment 718 (2020) 137302.
946 [47] D.R. Tree, K.I. Svensson, Soot processes in compression ignition engines, Prog. Energy Combust. Sci. 33(3)
947 (2007) 272-309.
948 [48] Z. Li, C. Song, J. Song, G. Lv, S. Dong, Z. Zhao, Evolution of the nanostructure, fractal dimension and size
949 of in-cylinder soot during diesel combustion process, Combust. Flame 158(8) (2011) 1624-1630.
950 [49] D. Kim, Y. Zhang, L. Clark, S. Kook, Y. Gao, In-Flame Soot Sampling and Morphology Analysis in an Optical
951 Spark-Ignition Direct-Injection (SIDI) Engine, SAE International Journal of Engines 11(6) (2018) 1007-1022.
952 [50] D. Kim, Y. Zhang, S. Kook, Influence of wall-wetting conditions on in-flame and exhaust soot structures in a
953 spark ignition direct injection petrol engine, International Journal of Engine Research (2020) 146808742091730.
954 [51] D. Kim, S. Kook, R. Kusakari, K. Shinohara, K. Iijima, T. Aizawa, Soot particles in piston-top pool fires and
955 exhaust at 5 and 15 MPa injection pressure in a gasoline direct-injection engine, Proceedings of the Combustion
956 Institute 38(4) (2021) 5761-5768.
957 [52] Y. Gao, D. Kim, Y. Zhang, S. Kook, M. Xu, Influence of ethanol blending ratios on in-flame soot particle
958 structures in an optical spark-ignition direct-injection engine, Fuel 248 (2019) 16-26.
959 [53] M. Potenza, M. Milanese, F. Naccarato, A. de Risi, In-cylinder soot concentration measurement by Neural
960 Network Two Colour technique (NNTC) on a GDI engine, Combustion and Flame 217 (2020) 331-345.
961 [54] E. Distaso, R. Amirante, P. Tamburrano, R.D. Reitz, Understanding the role of soot oxidation in gasoline
962 combustion: A numerical study on the effects of oxygen enrichment on particulate mass and number emissions in
963 a spark-ignition engine, Energy Conversion and Management 184 (2019) 24-39.
964 [55] T. Maruyama, Y. Sato, K. Endo, T. Tsukamoto, T. Aizawa, In-Cylinder GDI Soot via Visualization and Time-
965 Resolved Total Cylinder Sampling, SAE Technical Paper 2019-01-0037, 2019.
966 [56] C.J. Du, D.B. Kittelson, Total Cylinder Sampling from a Diesel Engine: Part III - Particle Measurements,
967 SAE Technical Paper 830243, 1983.
968 [57] J. Song, C. Song, Y. Tao, G. Lv, S. Dong, Diesel soot oxidation during the late combustion phase, Combust.
969 Flame 158(3) (2011) 446-451.

970 [58] N. Chen, C. Song, G. Lv, J. Song, J. Gao, Z. Zhang, Atom force microscopy analysis of the morphology,
971 attractive force, adhesive force and Young's modulus of diesel in-cylinder soot particles, Combust. Flame 162(12)
972 (2015) 4649-4659.
973 [59] J. Wei, C. Song, G. Lv, J. Song, L. Wang, H. Pang, A comparative study of the physical properties of in-
974 cylinder soot generated from the combustion of n-heptane and toluene/n-heptane in a diesel engine, P. Combust.
975 Inst. 35(2) (2015) 1939-1946.
976 [60] H. Seong, S. Choi, Oxidation-derived maturing process of soot, dependent on O2–NO2 mixtures and
977 temperatures, Carbon 93 (2015) 1068-1076.
978 [61] A. Messerer, R. Niessner, U. Pöschl, Comprehensive kinetic characterization of the oxidation and gasification
979 of model and real diesel soot by nitrogen oxides and oxygen under engine exhaust conditions: Measurement,
980 Langmuir–Hinshelwood, and Arrhenius parameters, Carbon 44(2) (2006) 307-324.
981 [62] Z. Hu, Z. Lu, H. Zhang, B. Song, Y. Quan, Effect of oxidation temperature on oxidation reactivity and
982 nanostructure of particulate matter from a China VI GDI vehicle, Atmospheric Environment 256 (2021) 118461.
983 [63] S. Choi, H. Seong, Oxidation characteristics of gasoline direct-injection (GDI) engine soot: Catalytic effects
984 of ash and modified kinetic correlation, Combustion and Flame 162(6) (2015) 2371-2389.
985 [64] J. Xing, L. Shao, R. Zheng, J. Peng, W. Wang, Q. Guo, Y. Wang, Y. Qin, S. Shuai, M. Hu, Individual particles
986 emitted from gasoline engines: Impact of engine types, engine loads and fuel components, Journal of Cleaner
987 Production 149 (2017) 461-471.
988 [65] H. Seong, S. Choi, N.J. Zaluzec, S. Lee, T. Wu, H. Shao, J.E. Remias, Identification of engine oil-derived ash
989 nanoparticles and ash formation process for a gasoline direct-injection engine, Environmental Pollution 272 (2021)
990 116390.
991 [66] A. Liati, D. Schreiber, P. Dimopoulos Eggenschwiler, Y. Arroyo Rojas Dasilva, A.C. Spiteri, Electron
992 microscopic characterization of soot particulate matter emitted by modern direct injection gasoline engines,
993 Combustion and Flame 166 (2016) 307-315.
994 [67] E. Kostenidou, A. Martinez-Valiente, B. R'Mili, B. Marques, B. Temime-Roussel, A. Durand, M. André, Y.
995 Liu, C. Louis, B. Vansevenant, D. Ferry, C. Laffon, P. Parent, B. D'Anna, Technical note: Emission factors,
996 chemical composition, and morphology of particles emitted from Euro 5 diesel and gasoline light-duty vehicles
997 during transient cycles, Atmospheric Chemistry and Physics 21(6) (2021) 4779-4796.
998 [68] J. Yang, P. Roth, C.R. Ruehl, M.M. Shafer, D.S. Antkiewicz, T.D. Durbin, D. Cocker, A. Asa-Awuku, G.
999 Karavalakis, Physical, chemical, and toxicological characteristics of particulate emissions from current technology
1000 gasoline direct injection vehicles, Science of the Total Environment 650(Pt 1) (2019) 1182-1194.
1001 [69] X. Zheng, S. Zhang, Y. Wu, G. Xu, J. Hu, L. He, X. Wu, J. Hao, Measurement of particulate polycyclic
1002 aromatic hydrocarbon emissions from gasoline light-duty passenger vehicles, Journal of Cleaner Production 185
1003 (2018) 797-804.
1004 [70] J.B. Heywood, Internal combustion engine fundamentals (Second Edition), McGraw-Hill Education, New
1005 York, 2018.
1006 [71] K.J. Baumgard, J.H. Johnson, The Effect of Fuel and Engine Design on Diesel Exhaust Particle Size
1007 Distributions, SAE Technical Paper 960131, 1996.
1008 [72] J. Gao, G. Tian, C. Ma, J. Chen, L. Huang, Physicochemical property changes during oxidation process for
1009 diesel PM sampled at different tailpipe positions, Fuel 219 (2018) 62-68.
1010 [73] B. Zielinska, Atmospheric transformation of diesel emissions, Experimental and Toxicologic Pathology 57
1011 (2005) 31-42.

[74] H.M. Oo, P. Karin, C. Charoenphonphanich, N. Chollacoop, K. Hanamura, Physicochemical characterization of direct injection Engines's soot using TEM, EDS, X-ray diffraction and TGA, Journal of the Energy Institute 96 (2021) 181-191.
[75] C. Wang-Hansen, P. Ericsson, B. Lundberg, M. Skoglundh, P.-A. Carlsson, B. Andersson, Characterization of Particulate Matter from Direct Injected Gasoline Engines, Topics in Catalysis 56(1-8) (2013) 446-451.
[76] G. Singh, Overview of the VTO Advanced Combustion Engine R&D Program, Annual Merit Review, 2016.
[77] C.K. Gaddam, Physical and Chemical Characterization of Gasoline Particulates and Differences Relative to Diesel Soot, Department of Energy and Mineral Engineering, The Pennsylvania State University, 2012.
[78] Z. Lu, S. Deng, X. Liu, L. Huang, R. Zhang, H. Song, G. Li, Morphology and composition of particles emitted from conventional and alternative fuel vehicles, Environmental Science and Pollution Research 28 (2021) 19810-19821.
[79] Z. Wu, C. Song, G. Lv, S. Pan, H. Li, Morphology, fractal dimension, size and nanostructure of exhaust particles from a spark-ignition direct-injection engine operating at different air–fuel ratios, Fuel 185 (2016) 709-717.
[80] D. Uy, M.A. Ford, D.T. Jayne, A.E. O'Neill, L.P. Haack, J. Hangas, M.J. Jagner, A. Sammut, A.K. Gangopadhyay, Characterization of gasoline soot and comparison to diesel soot: Morphology, chemistry, and wear, Tribology International 80 (2014) 198-209.
[81] H. Seong, K. Lee, S. Choi, Effects of Engine Operating Parameters on Morphology of Particulates from a Gasoline Direct Injection (GDI) Engine, SAE Technical Paper 2013-01-2574, 2013.
[82] R.L. Vander Wal, A.J. Tomasek, Soot nanostructure: dependence upon synthesis conditions, Combust. Flame 136(1-2) (2004) 129-140.
[83] C. Wang, H. Xu, J.M. Herreros, T. Lattimore, S. Shuai, Fuel Effect on Particulate Matter Composition and Soot Oxidation in a Direct-Injection Spark Ignition (DISI) Engine, Energy Fuels 28(3) (2014) 2003-2012.
[84] C.K. Gaddam, R.L. Vander Wal, Physical and chemical characterization of SIDI engine particulates, Combustion and Flame 160(11) (2013) 2517-2528.
[85] N. Sharma, A.K. Agarwal, Particle Characterization of Soot Aggregates Emitted by Gasohol Fueled Direct Injection Engine, Energy & Fuels 33(1) (2019) 420-428.
[86] Z. Zhang, W. Zhang, O.I. Awad, X. Ma, S. Pan, H. Xu, S. Shuai, Improved HRTEM image processing methods and the application on soot nanostructure analysis for GDI engine, Fuel 267 (2020) 116974.
[87] T. Lu, C.S. Cheung, Z. Huang, Effects of engine operating conditions on the size and nanostructure of diesel particles, J. Aerosol Sci 47 (2012) 27-38.
[88] X. Wang, Y. Wang, Y. Bai, P. Wang, D. Wang, F. Guo, Effects of 2,5-dimethylfuran addition on morphology, nanostructure and oxidation reactivity of diesel exhaust particles, Fuel 253 (2019) 731-740.
[89] S. Sakai, M. Hageman, D. Rothamer, Effect of Equivalence Ratio on the Particulate Emissions from a Spark-Ignited, Direct-Injected Gasoline Engine, SAE Technical Paper 2013-01-1560, 2013.
[90] K. Endo, Y. Sato, Y. Hojo, T. Maruyama, T. Tsukamoto, T. Aizawa, Morphology Analysis of Gasoline Engine Exhaust Particulates via Transmission Electron Microscopy, Transactions of Society of Automotive Engineers of Japan 51(5) (2020) 754-760.
[91] H. Seong, S. Choi, K. Lee, Examination of nanoparticles from gasoline direct-injection (GDI) engines using transmission electron microscopy (TEM), International Journal of Automotive Technology 15(2) (2014) 175−181.
[92] W. Zhang, C. Song, G. Lv, F. Bi, Y. Qiao, L. Wang, X. Zhang, Properties and oxidation of in-cylinder soot associated with exhaust gas recirculation (EGR) in diesel engines, Proceedings of the Combustion Institute 38(1)

(2021) 1319-1326.
[93] J. Jeon, N. Bock, D.B. Kittelson, W.F. Northrop, Correlation of nanoparticle size distribution features to spatiotemporal flame luminosity in gasoline direct injection engines, International Journal of Engine Research 21(7) (2020) 1107-1117.
[94] A. Zelenyuk, J. Wilson, D. Imre, M. Stewart, G. Muntean, J. Storey, V. Prikhodko, S. Lewis, M. Eibl, J. Parks, Detailed characterization of particulate matter emitted by lean-burn gasoline direct injection engine, International Journal of Engine Research 18(5-6) (2016) 560-572.
[95] J.E. Parks, J.M.E. Storey, V.Y. Prikhodko, M.M. Debusk, S.A. Lewis, Filter-based control of particulate matter from a lean gasoline direct injection engine, SAE Technical Paper 2016-01-0937, 2016.
[96] S. Shuai, X. Ma, Y. Li, Y. Qi, H. Xu, Recent Progress in Automotive Gasoline Direct Injection Engine Technology, Automotive Innovation 1(2) (2018) 95-113.
[97] C.M. Wang, H.M. Xu, J.M. Herreros, J.X. Wang, R. Cracknell, Impact of fuel and injection system on particle emissions from a GDI engine, Applied Energy 132 (2014) 178-191.
[98] S. Koch, H. Kubach, A. Velji, T. Koch, F.P. Hagen, H. Bockhorn, A. Loukou, D. Trimis, R. Suntz, Impact of the Injection Strategy on Soot Reactivity and Particle Properties of a GDI Engine, SAE Technical Paper 2020-01-0392, 2020.
[99] J.E. Easter, Influence of Fuel Introduction Parameters on the Reactivity and Oxidation Process of Soot from a Gasoline Direct Injection Engine, University of Michigan, 2018.
[100] Z. Xu, X. Li, C. Guan, Z. Huang, Effects of Injection Pressure on Diesel Engine Particle Physico-Chemical Properties, Aerosol Sci. Technol. 48(2) (2013) 128-138.
[101] U. Leidenberger, W. Mühlbauer, S. Lorenz, S. Lehmann, D. Brüggemann, Experimental Studies on the Influence of Diesel Engine Operating Parameters on Properties of Emitted Soot Particles, Combust. Sci. Technol. 184(1) (2012) 1-15.
[102] M. Potenza, M. Milanese, A. de Risi, Effect of injection strategies on particulate matter structures of a turbocharged GDI engine, Fuel 237 (2019) 413-428.
[103] Y. Choi, J. Lee, J. Jang, S. Park, Effects of fuel-injection systems on particle emission characteristics of gasoline vehicles, Atmospheric Environment 217 (2019) 116941.
[104] N. Sharma, A.K. Agarwal, Effect of the Fuel Injection Pressure on Particulate Emissions from a Gasohol (E15 and M15)-Fueled Gasoline Direct Injection Engine, Energy & Fuels 31(4) (2017) 4155-4164.
[105] C. Jiang, Z. Li, Y. Qian, X. Wang, Y. Zhang, X. Lu, Influences of fuel injection strategies on combustion performance and regular/irregular emissions in a turbocharged gasoline direct injection engine: Commercial gasoline versus multi-components gasoline surrogates, Energy 157 (2018) 173-187.
[106] X. He, M.A. Ratcliff, B.T. Zig, Effects of Gasoline Direct Injection Engine Operating Parameters on Particle Number Emissions, Energy & Fuels 26(4) (2012) 2014-2027.
[107] P. Eastwood, Particulate Emissions from Vehicles, John Wiley & Sons Ltd., England, 2008.
[108] J. Easter, S. Bohac, J. Hoard, A. Boehman, Influence of Ash-Soot Interactions on the Reactivity of Soot from a Gasoline Direct Injection Engine, Aerosol Science and Technology 54(12) (2020) 1373-1385.
[109] K. Miyashita, Y. Fukuda, Y. Shiozaki, K. Kondo, T. Aizawa, TEM Analysis of Soot Particles Sampled from Gasoline Direction Injection Engine Exhaust at Different Fuel Injection Timings, SAE Technical Paper 2015-01-1872, 2015.
[110] T.L. Barone, J.M.E. Storey, A.D. Youngquist, J.P. Szybist, An analysis of direct-injection spark-ignition (DISI) soot morphology, Atmospheric Environment 49 (2012) 268-274.

[111] Y. Kameya, K.O. Lee, Ultra-small-angle X-ray scattering characterization of diesel/gasoline soot: sizes and particle-packing conditions, Journal of Nanoparticle Research 15(10) (2013) 2006.
[112] M. Bogarra, J.M. Herreros, A. Tsolakis, A.P.E. York, P.J. Millington, F.J. Martos, Influence of on-board produced hydrogen and three way catalyst on soot nanostructure in Gasoline Direct Injection engines, Carbon 120 (2017) 326-336.
[113] S. Pan, Study on the Physicochemical Characteristics of Exhaust Particulates from Gasoline Direct Injection Engine, Tianjin University, 2012.
[114] J. Hwang, F. Sebastian Hirner, C. Bae, C. Patel, T. Gupta, A. Kumar Agarwal, HRTEM evaluation of primary soot particles originated in a small-bore biofuel compression-ignition engine, Appl. Therm. Eng. 159 (2019) 113899.
[115] M. Bogarra, J.M.M. Herreros-Arellano, A. Tsolakis, A.P.E. York, P. Millington, Reformate Exhaust Gas Recirculation (REGR) Effect on Particulate Matter (PM), Soot Oxidation and Three Way Catalyst (TWC) Performance in Gasoline Direct Injection (GDI) Engines, SAE International Journal of Engines 9(1) (2015) 305-314.
[116] M. Bogarra, J.M. Herreros, A. Tsolakis, J. Rodríguez-Fernández, A.P.E. York, P.J. Millington, Gasoline direct injection engine soot oxidation: Fundamentals and determination of kinetic parameters, Combustion and Flame 190 (2018) 177-187.
[117] M. Bogarra, J.M. Herreros, A. Tsolakis, A.P.E. York, P.J. Millington, F.J. Martos, Impact of exhaust gas fuel reforming and exhaust gas recirculation on particulate matter morphology in Gasoline Direct Injection Engine, Journal of Aerosol Science 103 (2017) 1-14.
[118] M. Hedge, P. Weber, J. Gingrich, T. Alger, I.A. Khalek, Effect of EGR on Particle Emissions from a GDI Engine, SAE International Journal of Engines 4(1) (2011) 650-666.
[119] K. Al-Qurashi, A.D. Lueking, A.L. Boehman, The deconvolution of the thermal, dilution, and chemical effects of exhaust gas recirculation (EGR) on the reactivity of engine and flame soot, Combust. Flame 158(9) (2011) 1696-1704.
[120] X. Li, Z. Xu, C. Guan, Z. Huang, Impact of exhaust gas recirculation (EGR) on soot reactivity from a diesel engine operating at high load, Appl. Therm. Eng. 68(1-2) (2014) 100-106.
[121] X. Li, Z. Xu, C. Guan, Z. Huang, Oxidative Reactivity of Particles Emitted from a Diesel Engine Operating at Light Load with EGR, Aerosol Sci. Technol. 49(1) (2014) 1-10.
[122] H. Liu, Z. Li, M. Zhang, H. Xu, X. Ma, S. Shuai, Exhaust non-volatile particle filtration characteristics of three-way catalyst and influencing factors in a gasoline direct injection engine compared to gasoline particulate filter, Fuel 290 (2021) 120065.
[123] H. Liu, Z. Li, H. Xu, X. Ma, S. Shuai, Nucleation mode particle evolution in a gasoline direct injection engine with/without a three-way catalyst converter, Applied Energy 259 (2020) 114211.
[124] A. Liati, P. Dimopoulos Eggenschwiler, D. Schreiber, V. Zelenay, M. Ammann, Variations in diesel soot reactivity along the exhaust after-treatment system, based on the morphology and nanostructure of primary soot particles, Combust. Flame 160(3) (2013) 671-681.
[125] R. Matarrese, Catalytic Materials for Gasoline Particulate Filters Soot Oxidation, Catalysts 11(8) (2021) 890.
[126] M.J. Kim, G.-H. Han, S.H. Lee, H.W. Jung, J.W. Choung, C.H. Kim, K.-Y. Lee, CeO2 promoted Ag/TiO2 catalyst for soot oxidation with improved active oxygen generation and delivery abilities, Journal of Hazardous Materials 384 (2020) 121341.
[127] L. Chen, J. Zhang, J. Wang, P. Chen, M. Fu, J. Wu, D. Ye, Insight into the Improvement Effect of Nitrogen

Dopant in Ag/Co3O4 Nanocubes for Soot Oxidation: Experimental and Theoretical Studies, Journal of Hazardous Materials 420 (2021) 126604.
[128] C. Liu, Z. Ma, Z. Yin, W. Du, E. Lv, Effect of Metallic GPF on the Micro Characteristics of Soot Particles of GDI Engine, International Journal of Automotive Technology 22(6) (2021) 1569-1578.
[129] M. Saffaripour, T.W. Chan, F. Liu, K.A. Thomson, G.J. Smallwood, J. Kubsh, R. Brezny, Effect of Drive Cycle and Gasoline Particulate Filter on the Size and Morphology of Soot Particles Emitted from a Gasoline-Direct-Injection Vehicle, Environmental Science & Technology 49(19) (2015) 11950-8.
[130] J. Yang, P. Roth, T.D. Durbin, K.C. Johnson, D.R. Cocker, 3rd, A. Asa-Awuku, R. Brezny, M. Geller, G. Karavalakis, Gasoline Particulate Filters as an Effective Tool to Reduce Particulate and Polycyclic Aromatic Hydrocarbon Emissions from Gasoline Direct Injection (GDI) Vehicles: A Case Study with Two GDI Vehicles, Environmental Science & Technology 52(5) (2018) 3275-3284.
[131] M. Munoz, R. Haag, K. Zeyer, J. Mohn, P. Comte, J. Czerwinski, N.V. Heeb, Effects of Four Prototype Gasoline Particle Filters (GPFs) on Nanoparticle and Genotoxic PAH Emissions of a Gasoline Direct Injection (GDI) Vehicle, Environmental Science & Technology 52(18) (2018) 10709-10718.
[132] Y. Wang, H. Liu, C.-F.F. Lee, Particulate matter emission characteristics of diesel engines with biodiesel or biodiesel blending: A review, Renewable and Sustainable Energy Reviews 64 (2016) 569-581.
[133] O.I. Awad, R. Mamat, T.K. Ibrahim, A.T. Hammid, I.M. Yusri, M.A. Hamidi, A.M. Humada, A.F. Yusop, Overview of the oxygenated fuels in spark ignition engine: Environmental and performance, Renewable and Sustainable Energy Reviews 91 (2018) 394-408.
[134] I.M. Yusri, R. Mamat, G. Najafi, A. Razman, O.I. Awad, W.H. Azmi, W.F.W. Ishak, A.I.M. Shaiful, Alcohol based automotive fuels from first four alcohol family in compression and spark ignition engine: A review on engine performance and exhaust emissions, Renewable and Sustainable Energy Reviews 77 (2017) 169-181.
[135] G.D.J. Guerrero Peña, Y.A. Hammid, A. Raj, S. Stephen, T. Anjana, V. Balasubramanian, On the characteristics and reactivity of soot particles from ethanol-gasoline and 2,5-dimethylfuran-gasoline blends, Fuel 222 (2018) 42-55.
[136] J.H. Chan, A. Tsolakis, J.M. Herreros, K.X. Kallis, C. Hergueta, S. Sittichompoo, M. Bogarra, Combustion, gaseous emissions and PM characteristics of Di-Methyl Carbonate (DMC)-gasoline blend on gasoline Direct Injection (GDI) engine, Fuel 263 (2020) 116742.
[137] X. Wang, Y. Wang, Y. Bai, Oxidation behaviors and nanostructure of particulate matter produced from a diesel engine fueled with n-pentanol and 2-ethylhexyl nitrate additives, Fuel 288 (2021) 119844.
[138] N. Serhan, A. Tsolakis, F.J. Martos, Effect of propylene glycol ether fuelling on the different physico-chemical properties of the emitted particulate matters: Implications of the soot reactivity, Fuel 219 (2018) 1-11.
[139] C. Hergueta, A. Tsolakis, J.M. Herreros, M. Bogarra, E. Price, K. Simmance, A.P.E. York, D. Thompsett, Impact of bio-alcohol fuels combustion on particulate matter morphology from efficient gasoline direct injection engines, Applied Energy 230 (2018) 794-802.
[140] N. Sharma, A.K. Agarwal, Particulate Morphology Characterization of Butanol–Gasoline Blend Fueled Spark-Ignition Direct Injection Engine, Journal of Energy Resources Technology 142(10) (2020) 102303.
[141] K.O. Lee, H. Seong, S. Sakai, M. Hageman, D. Rothamer, Detailed Morphological Properties of Nanoparticles from Gasoline Direct Injection Engine Combustion of Ethanol Blends, SAE Technical Paper 2013-24-0185, 2013.
[142] N. Sharma, R.A. Agarwal, A.K. Agarwal, Particulate Bound Trace Metals and Soot Morphology of Gasohol Fueled Gasoline Direct Injection Engine, Journal of Energy Resources Technology 141(2) (2019) 022201.

1180